Article

Cell Metabolism

Metformin Targets Mitochondrial Electron Transport to Reduce Air-Pollution-Induced Thrombosis

Graphical Abstract

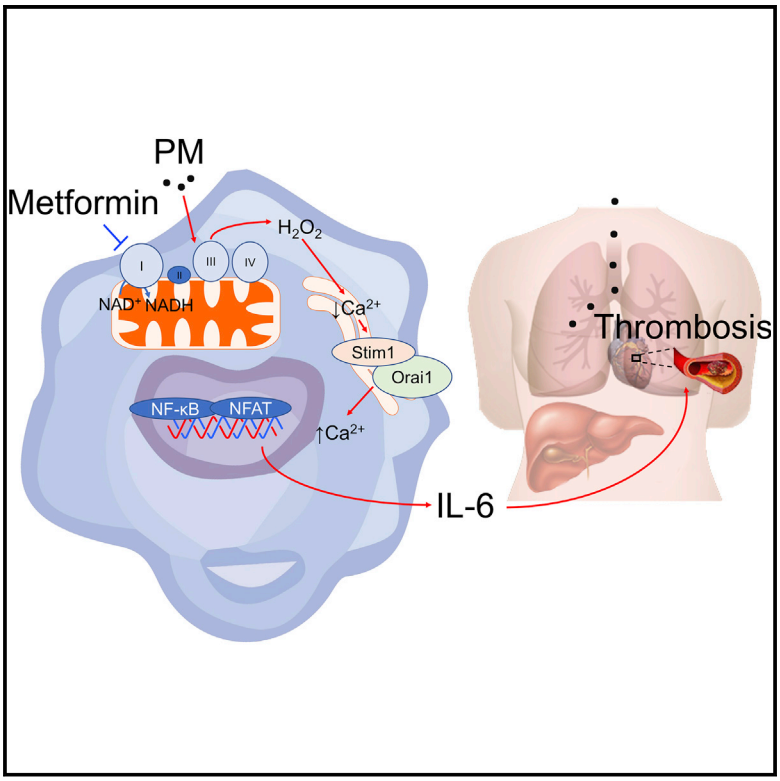

Authors

Saul Soberanes, Alexander V. Misharin, Amit Jairaman, ..., Navdeep S. Chandel, Gökhan M. Mutlu, G.R. Scott Budinger

Correspondence

gmutlu@medicine.bsd.uchicago.edu (G.M.M.),
s-buding@northwestern.edu (G.R.S.B.)

In Brief

Air pollution exposure has been linked to a variety of poor health outcomes, including an increased risk of death attributable to ischemic cardiovascular events. Soberanes et al. find that metformin may hold promise as a therapy, as its capacity to act as a mitochondrial complex I inhibitor prevents accelerated thrombosis in a murine model of particulate-matter inhalation.

Highlights

- Metformin prevents IL-6-dependent thrombosis induced by urban particulate matter
- Metformin inhibits mitochondrial complex I to prevent ROS-mediated IL-6 release
- Metformin inhibits mitochondrial ROS to prevent CRAC channel activation
- Mitochondrial ROS and CRAC channel inhibition *in vivo* prevent thrombosis

Soberanes et al., 2019, Cell Metabolism *29*, 1–13
January 8, 2019
https://doi.org/10.1016/j.cmet.2018.09.019

CellPress

Please cite this article in press as: Soberanes et al., Metformin Targets Mitochondrial Electron Transport to Reduce Air-Pollution-Induced Thrombosis, Cell Metabolism (2018), https://doi.org/10.1016/j.cmet.2018.09.019

Cell Metabolism
Article

Metformin Targets Mitochondrial Electron Transport to Reduce Air-Pollution-Induced Thrombosis

Saul Soberanes,[1,8] Alexander V. Misharin,[1,8] Amit Jairaman,[2] Luisa Morales-Nebreda,[1] Alexandra C. McQuattie-Pimentel,[1] Takugo Cho,[3] Robert B. Hamanaka,[3] Angelo Y. Meliton,[3] James M. Walter,[1] Ching-I Chen,[1] Monica Chi,[1] Stephen Chiu,[4] Francisco J. Gonzalez-Gonzalez,[1] Matthew Antalek,[5] Hiam Adbala-Valencia,[1] Sergio E. Chiarella,[1] Kaitlyn A. Sun,[3] Parker S. Woods,[3] Andrew J. Ghio,[6] Manu Jain,[1] Harris Perlman,[1] Karen M. Ridge,[1] Richard I. Morimoto,[5] Jacob I. Sznajder,[1] William E. Balch,[7] Sangeeta M. Bhorade,[1] Ankit Bharat,[4] Murali Prakriya,[2] Navdeep S. Chandel,[1] Gökhan M. Mutlu,[1,3,9,*] and G.R. Scott Budinger[1,9,10,*]

[1]Department of Medicine and Pulmonary and Critical Care Medicine, Northwestern University, 240 E Huron Street, M300, Chicago, IL 60611, USA
[2]Department of Pharmacology, Northwestern University, Chicago, IL 60611, USA
[3]Department of Medicine, University of Chicago, 5841 S Maryland Avenue, MC6026, Chicago, IL 60637, USA
[4]Department of Surgery, Northwestern University, Chicago, IL 60611, USA
[5]Rice Institute for Biomedical Research, Department of Molecular Biosciences, Northwestern University, Evanston, IL 60201, USA
[6]United States Environmental Protections Agency, Chapel Hill, NC 27599, USA
[7]Scripps Research, Department of Molecular Medicine, La Jolla, CA 92037, USA
[8]These authors contributed equally
[9]These authors contributed equally
[10]Lead Contact
*Correspondence: gmutlu@medicine.bsd.uchicago.edu (G.M.M.), s-buding@northwestern.edu (G.R.S.B.)
https://doi.org/10.1016/j.cmet.2018.09.019

SUMMARY

Urban particulate matter air pollution induces the release of pro-inflammatory cytokines including interleukin-6 (IL-6) from alveolar macrophages, resulting in an increase in thrombosis. Here, we report that metformin provides protection in this murine model. Treatment of mice with metformin or exposure of murine or human alveolar macrophages to metformin prevented the particulate matter-induced generation of complex III mitochondrial reactive oxygen species, which were necessary for the opening of calcium release-activated channels (CRAC) and release of IL-6. Targeted genetic deletion of electron transport or CRAC channels in alveolar macrophages in mice prevented particulate matter-induced acceleration of arterial thrombosis. These findings suggest metformin as a potential therapy to prevent some of the premature deaths attributable to air pollution exposure worldwide.

INTRODUCTION

Exposure to particulate matter air pollution is a major public health concern. In the developed world, it is estimated that lifespan would be extended for 0.8 years for every 10 $\mu g/m^3$ fall in the mean levels of particulate matter (PM) less than 2.5 μm in size, and exposure to PM was recently estimated to increase all-cause mortality in the United States Medicare Population by 7% (Di et al., 2017; Pope et al., 2009). In the developing world, the large number of urban dwellers and the very high levels of PM suggest effects of PM air pollution exposure on health are even more substantial (WHO Regional Office for Europe, 2013). While air pollution exposure has been linked to a variety of poor health outcomes, the major driver of mortality is an increased risk of death attributable to ischemic cardiovascular events, primarily heart attacks and ischemic/thrombotic strokes (Pope et al., 2009).

Urban PM air pollution consists of a core of ash or carbon decorated by organic molecules and metals that condense onto their surface during the combustion of fossil fuels (Nel, 2005). These latter features distinguish urban particulates from desert dust, volcanic ash, and wood smoke. To cope with life in dusty or smoky environments, mammals have evolved efficient mechanisms to clear ambient particles. For example, alveolar macrophages and mucociliary clearance efficiently clear carbon-based nanomaterials from the lungs to the larynx/feces with minimal or no inflammation (Duch et al., 2011; Semmler-Behnke et al., 2007). In contrast, we and others have shown that urban PM air pollution induces the release of pro-inflammatory cytokines, including interleukin-6 (IL-6) from alveolar macrophages before the particles are cleared. Alveolar macrophage-produced IL-6 enters the circulation to induce the transcription of several coagulation factors in the liver, and augments the tendency toward arterial thrombosis in a murine model of stroke—findings lacking in mice deficient in IL-6 (Chiarella et al., 2014; Mutlu et al., 2007). Key findings of this model were recently confirmed in humans in an interventional trial of filtered air compared with ambient air conducted in a region of China with high levels of ambient PM (Li et al., 2017). Accordingly, small molecules with acceptable risk profiles that can attenuate IL-6 release in response to PM in this model are predicted to lower the risk of arterial thrombosis in exposed populations.

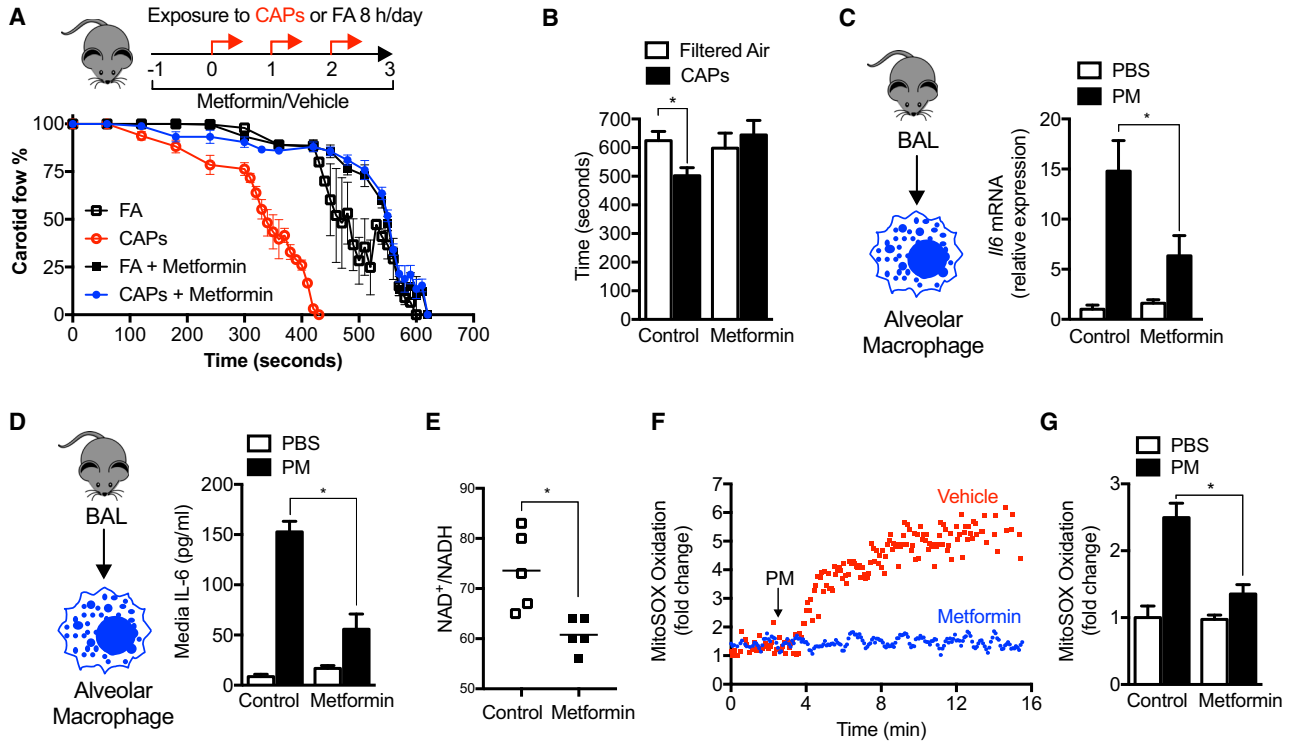

Figure 1. Metformin Prevents the Release of IL-6 and Enhanced Tendency to Thrombosis Induced by Exposure to Particulate Matter Air Pollution

(A) Mice were administered metformin in the drinking water (150 mg/kg/day) then exposed to concentrated ambient particulate matter air pollution <2.5 μm in diameter (CAPS) via inhalation in a versatile aerosol concentrator for 8 hr daily on three consecutive weekdays. At the end of the third day, a standardized ferric chloride injury was induced in the carotid artery and the time to thrombosis was assessed using an ultrasonic probe placed on the artery distal to the injury (n = 6, 5, 10, and 5 mice per condition, correspondingly, $p < 0.05$ for comparison with filtered air controls).

(B) Quantification of time to complete loss of blood flow after carotid artery injury (refers to A).

(C) Mice treated as in (A) were harvested for measurement of *Il6* mRNA in alveolar macrophages (n = 4 animals per condition, $^*p < 0.05$).

(D) Mice were treated with a standardized PM from the US National Institute of Standards and Technology (NIST) 10 μg/animal, intratracheally, and 24 hr later the levels of IL-6 in the BAL fluid (ELISA) were measured (n = 3 mice per condition, $^*p < 0.05$ for indicated comparison).

(E) Mice were treated with metformin in the drinking water for 24 hr and the levels of oxidized and reduced nicotinamide adenine dinucleotide (NAD^+/NADH) were measured in BAL fluid macrophages by mass spectroscopy (n = 5 animals per condition, $^*p < 0.05$).

(F) Alveolar macrophages from BAL fluid were allowed to adhere overnight to glass coverslips, loaded with the mitochondrially localized oxidant-sensitive dye MitoSOX (5 μM), and then exposed to PM containing perfusate (10 μg/mL) in the presence or absence of metformin (1 mM) on the stage of an epifluorescent microscope; oxidation of the dye was recorded from the same cellular region over time (a representative recording is shown).

(G) Quantification of MitoSOX oxidation (n = 3 mice per condition, $^*p < 0.05$); refers to (F).

See also Figure S1.

In animal models, metformin, a US Food and Drug Administration-approved drug for type 2 diabetes mellitus, slows the growth of tumors, prolongs lifespan, and reduces the risk of ischemic cardiovascular events (Martin-Montalvo et al., 2013; Maruthur et al., 2016; Wheaton et al., 2014). As a result, metformin is one of a handful of small molecules that are being considered as potential therapies to delay the onset of aging phenotypes in healthy people (Longo et al., 2015). Disruption of mitochondrial signaling by inhibition of complex I of the mitochondrial electron transport chain is a mechanism by which metformin slows tumor growth (Liu et al., 2016; Wheaton et al., 2014). Because the release of IL-6 and other pro-inflammatory cytokines in response to PM may require the generation of mitochondrial reactive oxygen species (ROS), we reasoned that metformin might reduce the risk of PM-induced thrombosis (Chiarella et al., 2014).

RESULTS

Metformin Prevents Increased Susceptibility to Arterial Thrombosis after Injury Induced by Exposure to PM

We treated mice with a therapeutic dose of metformin in their drinking water (100 mg/kg/day) beginning 24 hr before exposure to concentrated ambient PM (CAPs, $PM_{2.5}$) air pollution via inhalation (8 hr per day on three consecutive days). Metformin reduced the PM-induced acceleration of the time to carotid occlusion after ferric chloride-induced injury (a model of ischemic stroke) to a level that was similar to those measured in mice exposed to filtered air (Figures 1A and 1B). We have previously reported that the release of IL-6 from alveolar macrophages is necessary for this response (Mutlu et al., 2007). Accordingly, we measured the expression of the *Il6* gene in alveolar macrophages, which was reduced in the metformin-treated

animals (Figure 1C). Metformin inhibited PM-induced IL-6 protein release in response to PM in alveolar macrophages *ex vivo* (Figure 1D). Metformin also inhibited the PM-induced increase in IL-6 in bronchoalveolar lavage (BAL) fluid, in alveolar macrophages obtained from mice 24 hr after PM was administered intratracheally, and in a murine alveolar macrophage cell line (MHS) (Figures S1A–S1D).

Metformin Inhibits Electron Transport and PM-Induced Mitochondrial ROS Generation in Alveolar Macrophages

We assessed the ability of systemically administered metformin to inhibit mitochondrial respiration in alveolar macrophages by measuring the ratio of oxidized to reduced nicotinamide adenine dinucleotide (NAD^+/NADH) in alveolar macrophages immediately after their isolation. The ratio of NAD^+/NADH was significantly reduced in primary alveolar macrophages from mice treated with metformin in their drinking water when measured by mass spectroscopy or a colorimetric test (Figures 1E and S1E). To determine the role of metformin on the generation of mitochondrially derived ROS, we continuously measured the fluorescence of an oxidant-sensitive mitochondrially localized dye (MitoSOX) in primary murine alveolar macrophages on the stage of an epifluorescent microscope. Oxidation of the dye was observed within 2 min of adding PM to the perfusate and was reduced in cells pretreated with metformin before PM exposure (Figures 1F and 1G).

Metformin Prevents the Generation of Mitochondrial ROS to Reduce PM-Induced IL-6 Release

To determine whether metformin inhibits PM-induced mitochondrial ROS generation through its effects on complex I of the mitochondrial electron transport chain, we generated an alveolar macrophage cell line (MHS) stably transfected with lentiviral vectors encoding a yeast protein NDI1, which can transfer electrons from NADH to the ubiquinone pool without generating ROS and is insensitive to metformin (Figures S2A and S2B) (Wheaton et al., 2014). In contrast, mammalian complex I generates ROS and is sensitive to metformin (Bridges et al., 2014). Compared with control transfected cells, cells expressing NDI1 were resistant to metformin-induced inhibition of the basal oxygen consumption rate (OCR), PM-induced increases in mitochondrial ROS generation, and IL-6 production (Figures 2A–2C). A similar inhibition of PM-induced ROS generation and IL-6 release was observed in MHS cells treated with the complex I inhibitor piercidin A (Figures S2C and S2D). Unlike mammalian complex I, NDI1 is not capable of ROS generation, therefore, the ability to restore PM-induced mitochondrial ROS generation in NDI1 transfected cells suggested the generation of ROS downstream of complex I, most likely at complex III. Accordingly, we treated cells with a suppressor of superoxide production from mitochondrial complex III (S3QEL), which was identified through a chemical screen, and showed that this prevented PM-induced ROS generation and IL-6 release (Figures 2D and 2E) (Orr et al., 2015). In contrast, S1QEL, a suppressor of superoxide production from mitochondrial complex I identified in a similar screen, failed to prevent PM-induced ROS generation or IL-6 release (Figures 2D and 2E) (Brand et al., 2016). The less selective mitochondrial antioxidant Mito-TEMPO and the untargeted combined superoxide dismutase/catalase mimetic EUK-134 also prevented PM-induced mitochondrial ROS and IL-6 generation (Figures S2F and S2G). Together, these findings suggest that metformin inhibits mitochondrial ROS generation at complex III by reducing electron flow from the upstream complex I.

Many of the biological activities of metformin have been attributed to its ability to active AMPK independently or downstream of mitochondrial complex I inhibition (Ma et al., 2017). To determine if the inhibition of IL-6 generation by metformin was attributable to its ability to activate AMPK, we treated MHS cells with the AMPK activator A-769662. While both metformin and A-769662 activated AMPK, the AMPK activator had no effect on PM-induced IL-6 release from cells (Figures 2F and 2G). Similarly, when mice were treated with A-769662 at a dose shown to mimic the effects of metformin in a model of high-fat-induced atherosclerosis, we observed no change in the PM-induced increase in IL-6 in BAL fluid (Figure S2H) (Ma et al., 2017). To determine whether mitochondrial ROS generation alone was sufficient to induce IL-6 release from alveolar macrophages, we treated MHS cells with antimycin A, which blocks electron transport and increases ROS generation at complex III, or a modified version of paraquat that is targeted to the mitochondria (mito-paraquat), both titrated to induce similar oxidation of MitoSOX compared with PM (Figures 2H, S2I, and S2J). Neither agent alone induced IL-6 release; however, the addition of either antimycin A or mito-paraquat to a low dose of PM augmented IL-6 generation (Figure 2I). These results suggest that PM enhances the generation of mitochondrial ROS at complex III, which are necessary but not sufficient for PM-induced IL-6 release.

Metformin Inhibits PM-Induced Opening of Calcium-Release-Activated Ca^{2+} Channels

The rapidity of the oxidant response to PM prompted us to examine changes in intracellular calcium in response to PM. When primary alveolar macrophages were perfused with calcium-free medium and treated with PM, we observed a small increase in cytosolic calcium suggestive of endoplasmic reticulum calcium store depletion. Subsequent perfusion with calcium-replete medium was associated with a substantial increase in cytosolic calcium. Both of these responses were inhibited by metformin (Figure 3A). The increase in cytosolic calcium suggested that PM might promote opening of calcium-release-activated Ca^{2+} channels (CRAC). Indeed, the PM-induced increase in cytosolic calcium was inhibited by the CRAC channel inhibitors, Synta-66 and 2-2-aminoethoxydiphenyl borate (2-ABP) as well as the calcium chelator, 1,2-bis(o-aminophenoxy)ethane-N,N,N′,N′-tetraacetic acid (BAPTA) (Figure 3B). Treatment of primary murine alveolar macrophages with Synta-66 also attenuated PM-induced release of IL-6 (Figure 3C). Metformin did not inhibit store depletion or CRAC channel activation in response to thapsigargin (Figure S3A). Consistent with these findings, MHS cells stably transfected with lentiviruses encoding shRNAs targeting *Stim1* or *Orai1*, both components of the CRAC channel, showed reductions in PM-induced increases in intracellular calcium in calcium-replete medium, and reductions in PM-induced IL-6 release, compared with control transfected cells (Figures 3D–3F, S3C, and S3D).

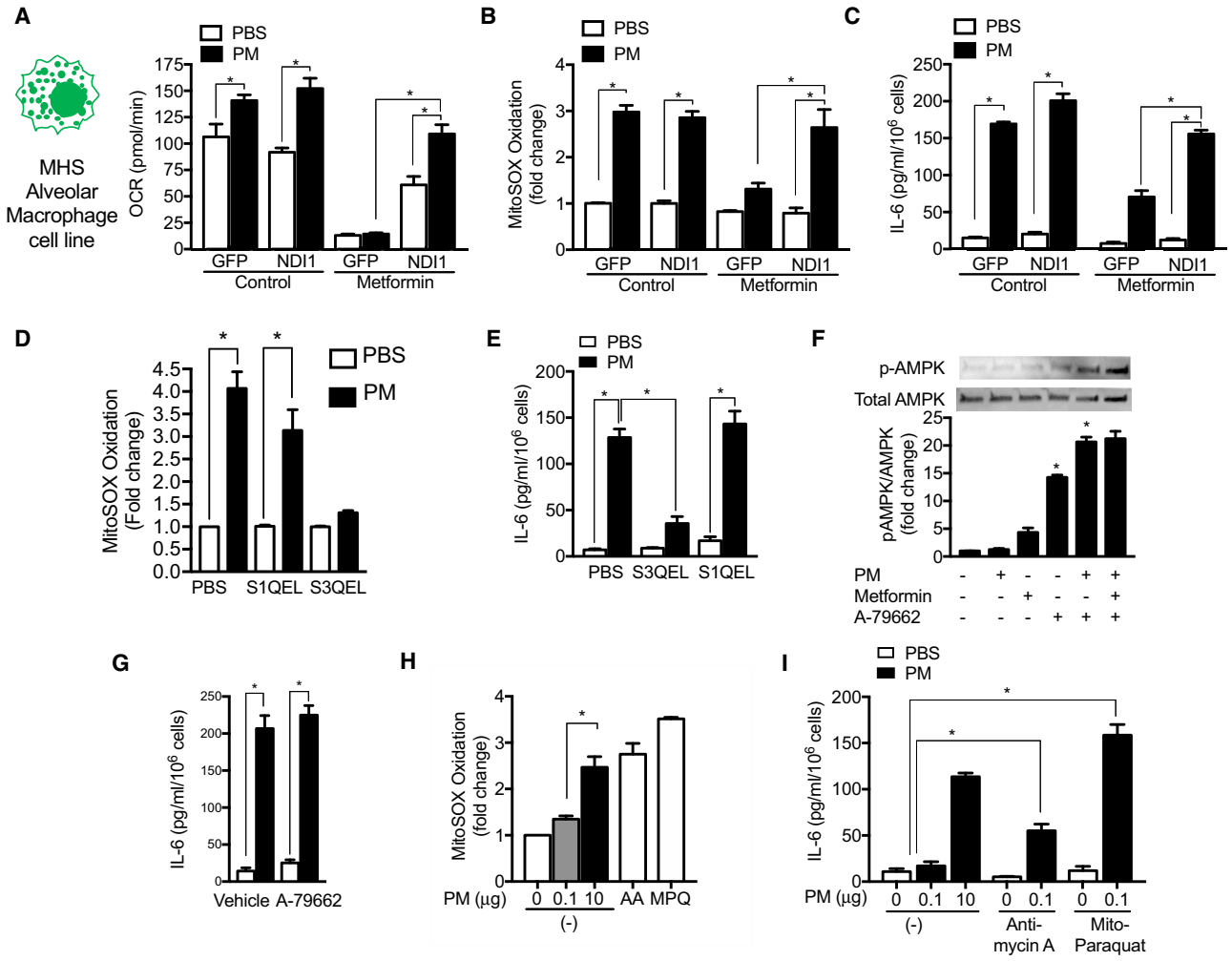

Figure 2. Metformin Inhibits Mitochondrial Electron Transport Complex I to Limit PM-Induced ROS Generation from Complex III

(A–C) A murine alveolar macrophage cell line (MHS) was stably transfected with a lentivirus encoding GFP and NDI1, a yeast protein capable of transferring electrons from NADH to complex II/III but incapable of ROS generation, or GFP alone. These cells were exposed to PM (10 μg/m^3) in the presence or absence of metformin and oxygen consumption (Seahorse XF Analyzer) (A) and the oxidation of MitoSOX (B) were measured 4 hr later; (C) the release of IL-6 into the medium was measured 24 hr later (minimum of eight replicates per measurement, *$p < 0.05$).

(D and E) MHS cells were treated with a suppressor of superoxide production from complex III (S3QEL) or complex I (S1QEL) (both at 5 μM) and mitochondrial ROS generation was measured (D) immediately after PM exposure as in (F); (E) IL-6 release was measured 4 hr later (n = 3, *$p < 0.05$).

(F and G) MHS cells were treated with a selective activator of AMPK A-79662 (2 μM) or vehicle and phosphorylation of AMPK (F) and PM-induced IL-6 release (G) were measured.

(H and I) MHS cells were treated with a dose of antimycin A (10 μM) or mitochondrially targeted paraquat (5 μM) selected to restore mitochondrial ROS to levels similar to PM alone, or in the presence of low dose PM, for measurement of MitoSOX oxidation (H, as in F) and IL-6 release (I) after 4 hr (n = 3–6 per condition, *$p < 0.01$).

See also Figure S2.

We have previously shown that PM-induced IL-6 release requires NF-κB activation and is augmented by cAMP response element binding protein (Chiarella et al., 2014). In other systems, CRAC channel activation enhances inflammatory gene expression through the activation of nuclear factor of activated T cells (NFAT) (Jairaman et al., 2015, 2016). Consistent with this mechanism, pretreatment of MHS cells with the calcineurin inhibitor cyclosporine A attenuated PM-induced IL-6 release without affecting PM-induced ROS generation or calcium release (Figures S3E–S3G).

Exposure to Particulate Matter Air Pollution Induces the Opening of CRAC Channels Downstream of Mitochondrial ROS Generation

Treatment of MHS cells with Synta-66 before PM administration or knockdown of *Orai1* did not affect PM-induced MitoSOX oxidation, suggesting the effects of PM on mitochondrial ROS generation are independent of CRAC channel opening (Figure 4A). Metformin inhibited the PM-induced increase in cytosolic calcium in MHS cells transfected with a control vector, but not in MHS cells that stably expressed NDI1 (Figures 4B

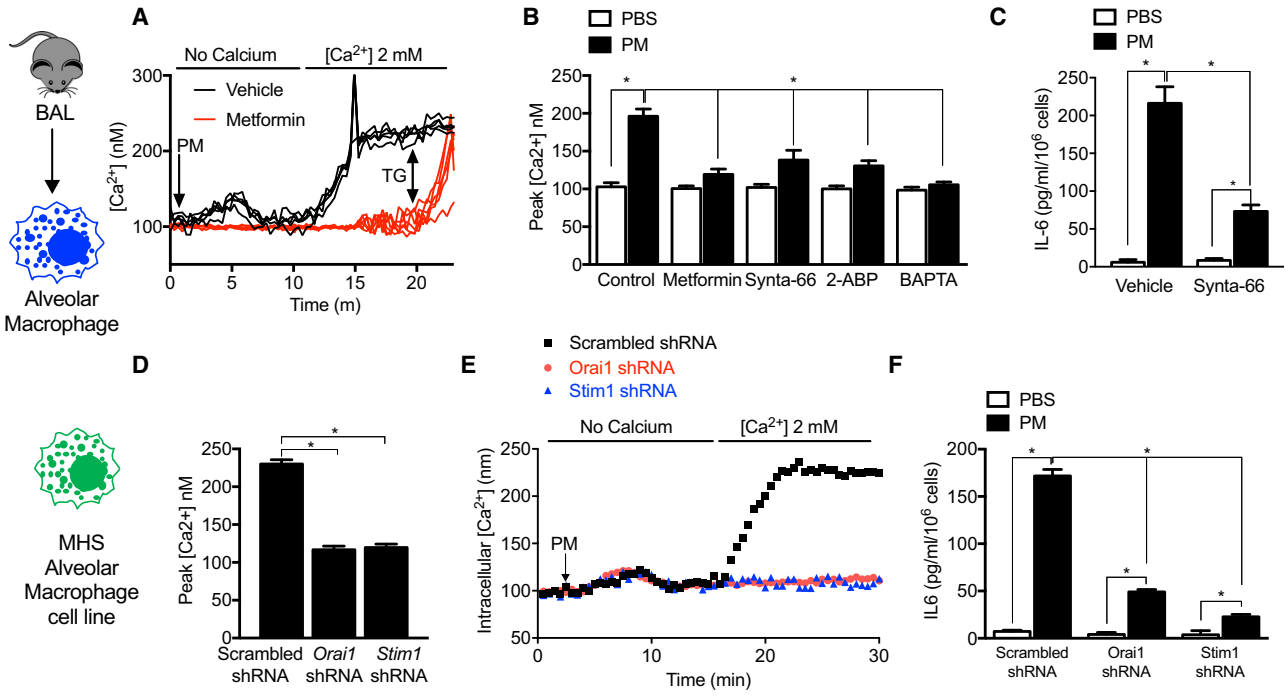

Figure 3. Store-Operated Calcium Channels Contribute to PM-Induced IL-6 Release

(A and B) Primary alveolar macrophages isolated from wild-type mice were allowed to adhere to glass coverslips before loading with the calcium sensitive dye Fura-2 (2 μM) and treated with PM in calcium-free medium followed by calcium-replete (2 mM) medium (A) after 1 hr pretreatment with metformin (1 mM), Synta-66 (10 μM), 2-aminoethoxydiphenyl borate (2-ABP, 10 μM), or 1,2-bis(o-aminophenoxy)ethane-N,N,N′,N′-tetraacetic acid (BAPTA, 10 μM) and the change in intracellular calcium concentration (B) in response to extracellular calcium was recorded (n = 3–4 mice per condition, *p < 0.05 for comparison with PM-treated cells).

(C) Primary alveolar macrophages from wild-type mice were pretreated for 1 hr with the CRAC channel inhibitor Synya-66 (10 μM) and then treated with PM (10 μg/cm^2), and the level of IL-6 in the medium was measured 24 hr later (n = 3).

(D–F) MHS cells were stably transfected with lentiviruses encoding shRNA against *Stim1*, *Orai1*, or a scrambled shRNA and treated with vehicle or PM (10 μg/cm^2). (D and E) The change in intracellular calcium was measured as in (A); (F) the level of IL-6 in the medium was measured 24 hr after PM treatment. *p < 0.05. See also Figure S3.

and 4C). These results suggest that metformin prevents CRAC channel opening in response to PM via its ability to inhibit mitochondrial ROS generation. Indeed, administration of S3QEL or the complex I inhibitor piercidin A prevented the PM-induced increases in cytosolic calcium (Figures 4D, 4E, and S4A), further suggesting calcium signaling occurred downstream of mitochondrial ROS generation.

Calcium store depletion induced by mitochondrially generated ROS might result from the activation of phospholipase-C (PLC) in the membrane, the inhibition of sarco/endoplasmic reticulum Ca^{2+}-ATPases, or an increase in the leak of calcium from the endoplasmic reticulum to the cytosol. Accordingly, we treated MHS cells with the PLC inhibitor U73122 and found it prevented PM-induced store depletion, CRAC channel activation, and IL-6 release, while the inactive control compound had no effect (Figures 4F–4H) (Hofmann et al., 1999). These effects occurred downstream of mitochondrial ROS generation as PM-induced mitochondrial ROS generation was unaffected by U73122 (Figure 4I). To determine whether mitochondrial ROS generation was sufficient to induce store depletion and activate CRAC channels, we treated cells with antimycin A or mito-paraquat, which alone did not activate CRAC channels (Figures S4B and S4C).

Genetic Deletion of Mitochondrial Electron Transport Prevents the Increase in IL-6 in Response to PM

The intratracheal administration of PM did not induce the recruitment of inflammatory cells to the lung, suggesting tissue-resident alveolar macrophages are responsible for the acute effects of PM *in vivo* (Figures S5A and S5B). This allowed us to determine the importance of mitochondrial ROS generation in the response to PM *in vivo* by generating mice lacking the nuclear-encoded mitochondrial transcription factor A (TFAM) in macrophages ($Cre^{CD11c}/Tfam^{flox/flox}$). TFAM is a nuclear-encoded gene that is required for the transcription of genes encoded by mitochondrial DNA, including 13 genes that encode necessary components of most complexes within the electron transport chain (Fisher et al., 1992). Flow sorting of myeloid cell populations of 8- to 12-week-old $Cre^{CD11c}/Tfam^{flox/flox}$ and $Tfam^{flox/flox}$ mice showed similar numbers of alveolar macrophages and other myeloid cell populations in the lung and no obvious morphologic changes (Figure S5C). Flow-sorted alveolar macrophages from $Cre^{CD11c}/Tfam^{flox/flox}$ exhibited reduced levels of *Tfam* mRNA while these levels were normal in neutrophils (Figure 5A). When we treated $Cre^{CD11c}/Tfam^{flox/flox}$ mice with PM intratracheally, the acceleration of carotid thrombosis in response to PM was attenuated, and BAL fluid levels of IL-6 were reduced compared with

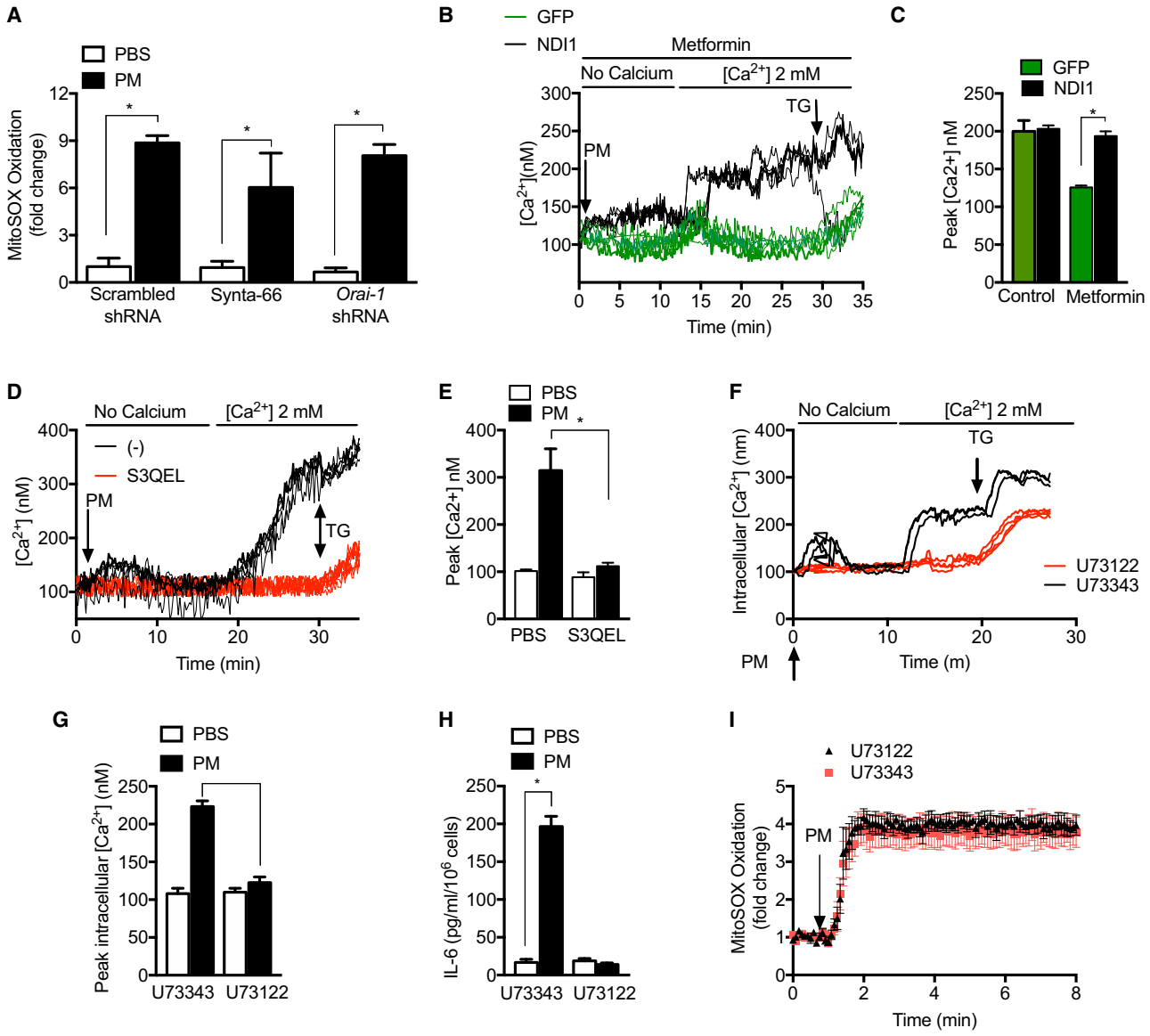

Figure 4. PM-Induced CRAC Channel Activation Occurs Downstream of Mitochondrial ROS Generation

(A) MHS cells were stably transfected with lentiviruses encoding shRNA against *Stim1* or *Orai1* or a scrambled shRNA and treated with vehicle or PM (10 μg/cm^2) and the oxidation of MitoSOX dye was measured (n = 3, *p < 0.05).

(B) MHS cells transfected with GFP or GFP-NDI1 were treated with PM with or without metformin (1 mM) and changes in intracellular calcium upon the addition of calcium-replete medium were measured. A representative tracing is shown. Thapsigargin (TG) (25 nM) was added to the cells at the end of each experiment. See also Figure S4.

(C) Peak calcium measures after the addition of calcium-replete medium in cells treated with PM with or without metformin (1 mM) (n = 3, *p < 0.05); refers to (B).

(D) MHS cells were treated with S3QEL (5 μM) 1 hr before treatment with PM (10 μg/cm^3) and immediate changes in intracellular calcium and IL-6 release into the media after 24 hr were measured. A representative tracing is shown. Thapsigargin (TG) (25 nM) was added to the cells at the end of each experiment. See also Figure S4.

(E) Peak calcium measurements after the addition of calcium-replete medium (n = 3, *p < 0.05); refers to (D).

(F) MHS cells were pretreated for 1 hr with the PLC inhibitor U73122 or the inactive control compound U73343 (both 200 nM), and changes in intracellular calcium upon the addition of calcium-replete medium were measured. A representative tracing is shown. Thapsigargin (TG) (25 nM) was added to the cells at the end of each experiment.

(G) Peak calcium measurements after the addition of calcium-replete medium (n = 3, *p < 0.05); refers to (F).

(H) MHS cells were pretreated for 1 hr with the PLC inhibitor U73122 or the inactive control compound U73343 (both 200 nM), and IL-6 release (24 hr) was measured. (n = 3, *p < 0.05).

(I) MHS cells were pretreated for 1 hr with the PLC inhibitor U73122 or the inactive control compound U73343 (both 200 nM), and MitoSOX oxidation was measured. (n = 3, mean results with SEM are shown).

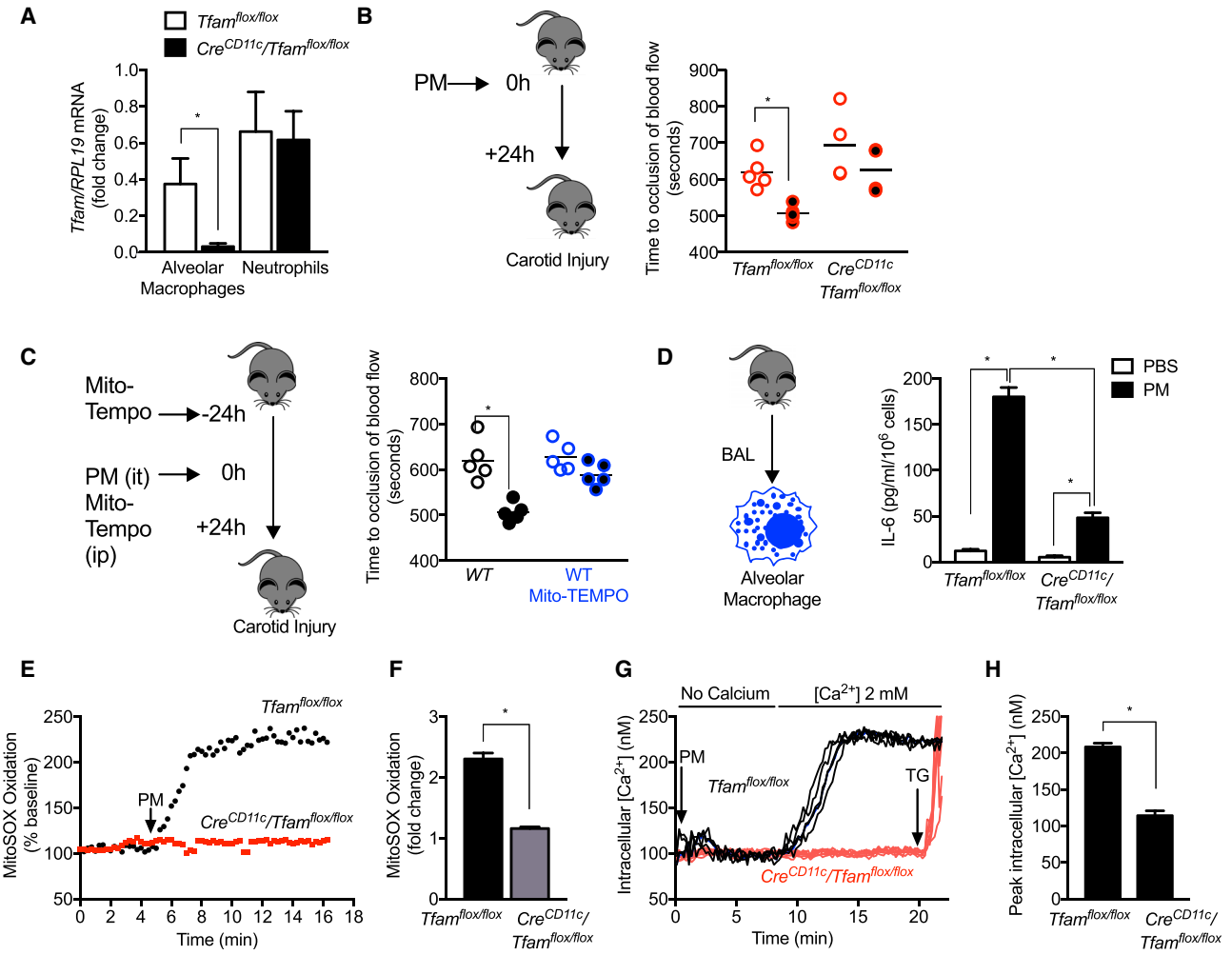

Figure 5. Mitochondrial Electron Transport Is Necessary for the PM-Induced Acceleration of Carotid Thrombosis

Mice deficient in *Tfam*, a nuclear-encoded transcription factor necessary for mitochondrial DNA transcription, in alveolar macrophages ($Cre^{CD11c}/Tfam^{flox/flox}$) were compared with control mice.

(A) Levels of *Tfam* mRNA in flow-sorted alveolar macrophages and neutrophils. See also Figure S5.

(B) Mice were treated with PBS or PM (10 μg, intratracheally) and 24 hr later, the time to cessation of carotid artery blood flow after a standardized ferric chloride injury was measured.

(C) Wild-type C57BL/6 mice were treated with the mitochondrially targeted antioxidant Mito-TEMPO (0.7 mg/kg/day, intraperitoneally) 24 hr before and simultaneously with the administration of PM (10 μg/mouse) or PBS, and the time to cessation of carotid artery blood flow after standardized ferric chloride injury was measured.

(D) Primary alveolar macrophages from the indicated strains of mice were treated with PM and IL-6 levels in the medium were measured 24 hr later (n = 3).

(E) Primary alveolar macrophages from the indicated strains were loaded with MitoSOX, and mitochondrial ROS generation was measured continuously after the administration of PM on the stage of an epifluorescent microscope. A representative tracing is shown.

(F) Increase in MitoSOX oxidation after the addition of PM (n = 4, *p < 0.05); refers to (E).

(G) Primary alveolar macrophages were loaded with Fura-2 for measurement of intracellular calcium levels after PM exposure in calcium-free medium followed by calcium-replete medium. Representative tracings are shown. Thapsigargin (TG) (25 nM) was added to the cells at the end of each experiment.

(H) Peak calcium measures after the addition of calcium-replete medium (n = 3, *p < 0.05) refers to (G).

$Tfam^{flox/flox}$ controls (Figure 5B). To confirm our *in vitro* findings suggesting mitochondrial ROS were required for the generation of IL-6 in response to PM, we treated mice with Mito-TEMPO subcutaneously beginning 1 day before PM exposure. Treatment with Mito-TEMPO also prevented PM-induced thrombosis (Figure 5C). Consistent with these findings, IL-6 levels were reduced in primary alveolar macrophages isolated by BAL from $Cre^{CD11c}/Tfam^{flox/flox}$ mice compared with those from $Tfam^{flox/flox}$ mice (Figure 5D). Similarly, alveolar macrophages from $Cre^{CD11c}/Tfam^{flox/flox}$ mice failed to generate ROS or increase intracellular calcium in response to PM (Figures 5E–5H).

Genetic Deletion of *Orai1* in Alveolar Macrophages Prevents the Increase in IL-6 in Response to PM

We used a similar strategy to examine the importance of CRAC channel activation in the response to PM *in vivo*.

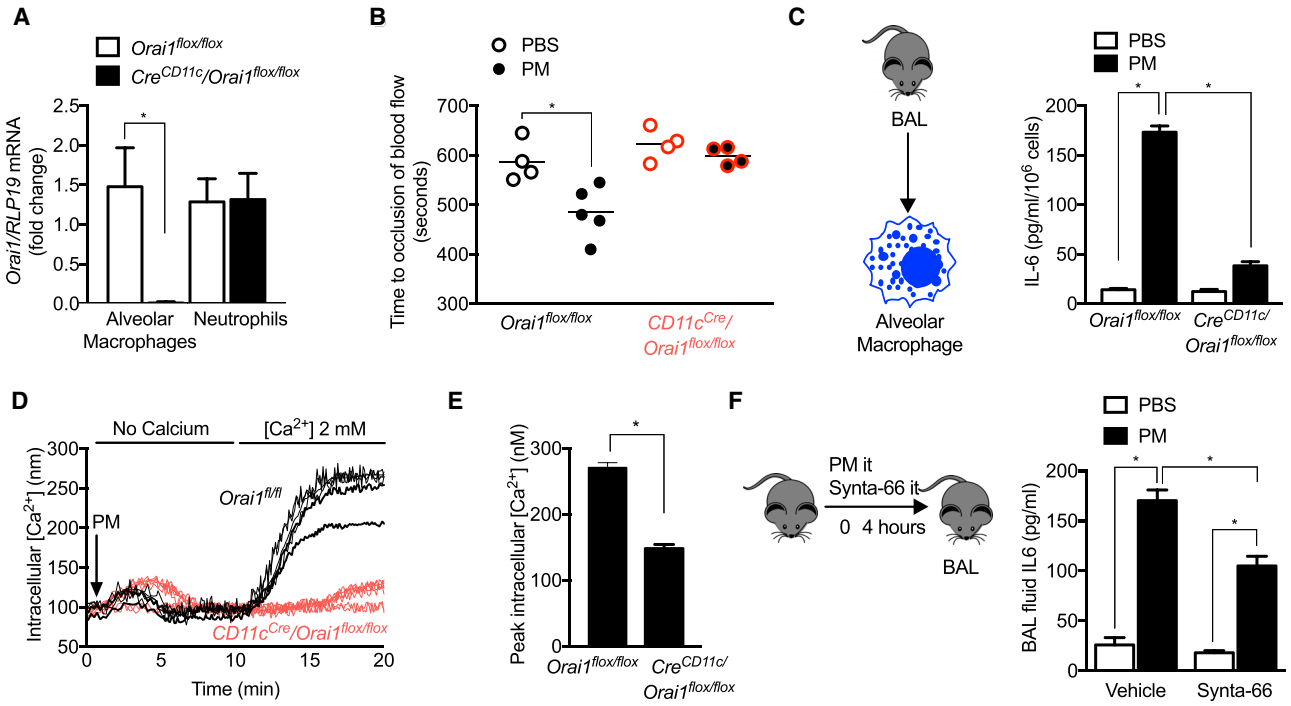

Figure 6. CRAC Channel Activation Is Necessary for PM-Induced Acceleration of Carotid Thrombosis

(A) Levels of *Orai1* mRNA in flow-sorted alveolar macrophages and neutrophils from mice deficient in *Orai1*, a necessary component of CRAC channels, in alveolar macrophages. (n = 3, *p < 0.05).

(B) Mice were treated with PBS or PM (10 μg, intratracheally), and 24 hr later, the time to cessation of carotid artery blood flow after a standardized ferric chloride injury was measured in $Orai1^{flox/flox}$ mice and $Cre^{CD11c}/Orai1^{flox/flox}$ mice (n = 4, *p < 0.05).

(C) Primary alveolar macrophages were treated with PM and the levels of IL-6 were measured 24 hr later (n = 3, *p < 0.05).

(D) Primary alveolar macrophages were loaded with Fura-2 for measurement of intracellular calcium levels after PM exposure in calcium-free medium followed by calcium-replete medium. Representative tracings are shown. Thapsigargin (TG) (25 nM) was added to the cells at the end of each experiment.

(E) Peak calcium measurements after the addition of calcium-replete medium (n = 3, *p < 0.05); refers to (D).

(F) Wild-type mice were treated with Synta-66 (10 μM) intratracheally or vehicle simultaneous with the intratracheal instillation of PM (10 μg/mouse) and the levels of IL-6 in the BAL were measured 6 hr later (n = 3, *p < 0.05).

Orai1 was efficiently deleted in alveolar macrophages from $CD11c^{Cre}/Orai1^{flox/flox}$ animals compared with $Orai1^{flox/flox}$ controls (Figure 6A). The acceleration of carotid thrombosis induced by the intratracheal administration of PM in $Orai1^{flox/flox}$ controls was absent in $CD11c^{Cre}/Orai1^{flox/flox}$ mice (Figure 6B). Primary alveolar macrophages from $Cre^{CD11c}/Orai1^{flox/flox}$ mice showed reduced levels of IL-6 production and intracellular calcium release in response to PM compared with those from $Orai1^{flox/flox}$ mice (Figures 6C–6E). Consistent with these findings, the intratracheal administration of Synta-66 to mice simultaneously with the instillation of PM was associated with reduced levels of IL-6 in the BAL fluid 4 hr later (Figure 6F). These findings are of interest as the loss of CRAC channels was previously reported to induce no phenotypic changes in alveolar macrophages (Vaeth et al., 2015).

Metformin Prevents PM-Induced ROS Generation, CRAC Channel Activation, and IL-6 Production in Human Macrophages

Our data suggest that PM induces the generation of mitochondrial ROS, which augment IL-6 release by activating CRAC channels. To confirm the potential importance of these findings in humans, we measured mitochondrial ROS generation and calcium levels in primary human alveolar macrophages obtained from healthy donors after treatment with metformin and/or Synta-66. Consistent with our findings in murine alveolar macrophages, metformin inhibited mitochondrial ROS generation, calcium release, and IL-6 release after PM exposure (Figures 7A–7D). As our results suggested that metformin acts to limit mitochondrial ROS and calcium-mediated activation of IL-6, we reasoned it would likely affect other processes in alveolar macrophages triggered by exposure to PM. Therefore, mice were treated in the drinking water with metformin for 24 hr before we instilled PM intratracheally. Alveolar macrophages were flow sorted from whole-lung homogenates 24 hr later for transcriptomic analysis (RNA-seq) and metabolomic analysis. Metformin treatment resulted in significant changes in the measured metabolites in alveolar macrophages, including reductions in glycolytic and tricarboxylic acid cycle intermediates, as well as high-energy phosphates, with little change in amino acids (Figure S6). While the overall change in metabolites was highly significant ($p < 0.001$ by ANOVA), individual metabolites did not reach significance after corrections for multiple comparisons

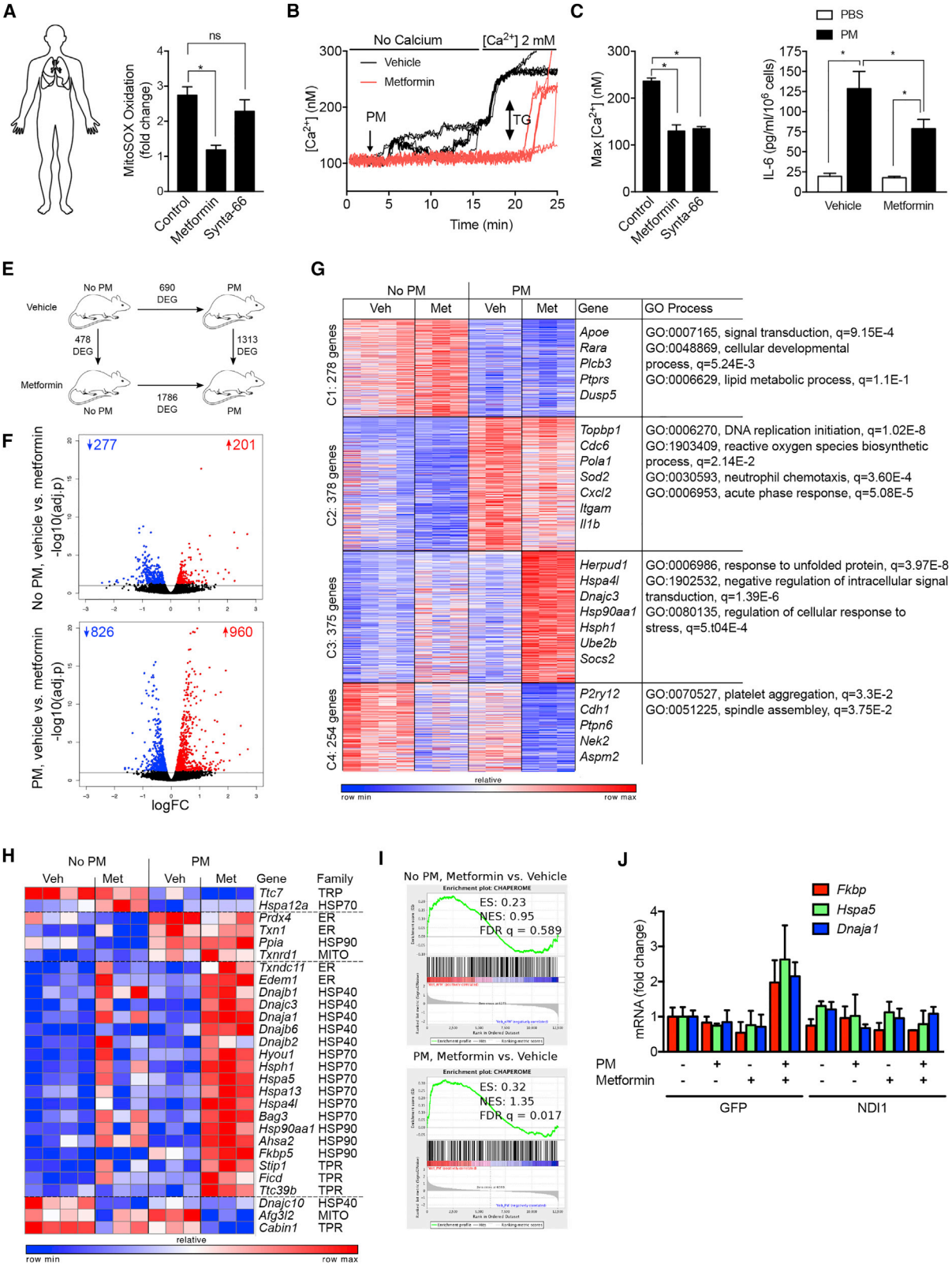

(legend on next page)

(false discovery rate [FDR] $p < 0.05$) (Table S1). Metformin treatment alone had a relatively minor effect on gene expression in alveolar macrophages in the steady state (476 differentially expressed genes, FDR $p < 0.05$), but the response to PM exposure differed substantially when compared with untreated animals (1,313 differentially expressed genes, FDR $p < 0.05$) (Figures 7E and 7F, Table S1). To better understand the changes induced by PM and metformin, we performed k-means clustering of the 1,285 differentially expressed genes identified by an ANOVA-like test, FDR $p < 0.001$ (Figure 7G, Table S1). Genes downregulated after PM exposure (cluster 1) include those related to signal transduction and the cellular developmental process. Consistent with our findings, the genes upregulated in response to PM and relatively downregulated by metformin (cluster 2) included ROS biosynthetic process, neutrophil chemotaxis, and the acute phase response. Genes that were downregulated upon administration of PM and metformin (cluster 4) were associated with platelet aggregation and cell division (spindle assembly).

Surprisingly, many of the genes that were upregulated in response to PM and metformin treatment compared with PM treatment alone (cluster 3) were related to the unfolded protein response, negative regulation of intracellular signal transduction, and regulation of the response to stress. These findings suggest metformin induces a stress response that could indirectly suppress inflammatory signaling. To explore this hypothesis further, we examined the expression of a curated list of chaperone proteins in our dataset, which showed that many genes identified as human chaperones were upregulated in alveolar macrophages from metformin- and PM-treated animals (Figure 7H). We confirmed upregulation of chaperone genes using gene set enrichment analysis (enrichment score 0.32, FDR $p = 0.017$, Figure 4I) (Subramanian et al., 2005; Brehme et al., 2014). Using MHS cells transfected with NDI1, we showed that the increase in selected chaperones in metformin- and PM-treated cells was dependent on the ability of metformin to inhibit complex I (Figure 7J.). These data suggest the intriguing hypothesis that complex I inhibition by metformin may also attenuate inflammatory signaling pathways indirectly by triggering global cellular stress response pathways that protect against macromolecular damage.

DISCUSSION

We found that the commonly used drug metformin can attenuate PM-induced IL-6 release from alveolar macrophages and reduce the resulting increase in the risk of arterial thrombosis after injury. Metformin acted as a complex I inhibitor in alveolar macrophages to reduce mitochondrial ROS from complex III of the mitochondrial electron transport chain in response to PM. In alveolar macrophages from mice and humans, PM-induced mitochondrial ROS generation caused endoplasmic reticulum calcium store depletion, and the opening of store-operated calcium channels, which augmented IL-6 release. Mitochondrial ROS alone were insufficient to induce store depletion or IL-6 release but acted in concert with particles to augment these responses. Our results provide genetic evidence *in vivo* to support the importance of signaling by mitochondrial ROS and CRAC channels in the release of IL-6 from alveolar macrophages and in the accelerated thrombosis after carotid artery injury induced by PM air pollution exposure.

In a murine alveolar macrophage-like cell line, we could restore PM-induced signaling events by overexpressing the yeast protein NDI1, which can transfer electrons from NADH to the ubiquinone pool but cannot generate ROS and is insensitive to metformin (Seo et al., 1998). Using small molecules that suppress superoxide production specifically at complex III or complex I, we show that NDI1 restores electron flux to complex III to restore mitochondrial ROS generation. These data are consistent with previous studies showing that metformin inhibits the generation of ROS induced by reverse electron transport (Batandier et al., 2006; Bridges et al., 2014). An interesting aspect

Figure 7. Metformin Prevents PM-Induced IL-6 Release from Primary Human Alveolar Macrophages and Modifies Transcriptional Response to PM in Murine Alveolar Macrophages

(A) Flow-sorted alveolar macrophages were isolated from biopsies from donor lungs obtained at the time of lung transplantation and allowed to adhere to glass coverslips for 4–8 hr. The cells were loaded with MitoSOX (5 μM) and then pretreated with saline, metformin (1 mM), or Synta-66 (10 μM) prior to treatment with PM (10 $\mu g/cm^2$) for measurement of mitochondrial ROS generation.

(B) Alveolar macrophages were allowed to adhere to glass coverslips prior to loading with Fura-2 (2 μM) and then treated with metformin (1 mM) or saline 1 hr before treatment with PM, and intracellular calcium levels were measured in calcium-free medium followed by calcium-replete medium (1 mM). Representative tracings are shown. Thapsigargin (TG, 25 nM) was added at the end of the experiment.

(C) Peak calcium measurements after the addition of calcium-replete medium (data from four subjects, *$p < 0.05$); refers to (B).

(D) Primary human alveolar macrophages were treated with metformin (1 mM) 1 hr before treatment with PM (10 $\mu g/cm^2$), and IL-6 levels in the medium were measured 4 hr later.

(E) Mice were treated with metformin in the drinking water for 24 hr before and after instilling PM (10 μg/mouse) intratracheally, and alveolar macrophages flow sorted from whole-lung homogenates 24 hr later were subjected to transcriptional profiling via RNA-seq. Schematic of the experimental design is shown. Numbers indicate differentially expressed genes (FDR $p < 0.05$). See also Figure S6.

(F) Volcano plots demonstrating up- and downregulated genes in mice treated with metformin before and after exposure to PM, numbers indicate up- and downregulated genes (FDR $p < 0.05$); refers to (E).

(G) k-means clustering identifies metformin-specific clusters of genes. Differentially expressed genes (1,285 genes, identified using ANOVA-like tests implemented in the edgeR package, FDR $p < 0.001$) in alveolar macrophages exposed to PM in the presence and absence of metformin pretreatment *in vivo* were subjected to k-means clustering (number of genes per cluster is shown on the left). Representative gene names and gene ontology processes for each cluster are shown on the right.

(H) Chaperones upregulated in mice treated with metformin and then exposed to PM. Individual genes and chaperone family shown.

(I) Gene set enrichment analysis shows enrichment for chaperone genes after treatment with metformin that is more significant in alveolar macrophages from PM-exposed mice.

(J) MHS cells stably transfected with a lentivirus encoding NDI1 or a control lentivirus (GFP) were treated with PM, and the levels of mRNA encoding the indicated genes were measured 24 hr later using RT-qPCR ($n = 3$).

of our study is the relationship between mitochondrial ROS and calcium release. Our findings using inhibitors implicate the activation of PLC in the store depletion induced by mitochondrial ROS upon PM exposure, but additional studies are required to better understand these pathways.

Inhibition of electron transport by metformin activates AMPK, which is proposed as a mechanism for its antidiabetic effects. Our finding that mitochondrially targeted antioxidants mimicked the effects of metformin *in vitro* and *in vivo* argue against a direct role for electron transport inhibition or AMPK activation in this protection. Furthermore, when we treated primary alveolar macrophages or mice with a direct activator of AMPK, PM-induced IL-6 release was unaffected. Unbiased transcriptional profiling of alveolar macrophages from metformin-treated animals using RNA-seq showed only small differences between metformin-treated and untreated animals, however, there were marked differences in their response to PM. Specifically, alveolar macrophages from metformin-treated animals showed a significant upregulation of chaperone genes involved in proteostasis in response to PM when compared with untreated control animals. Using an alveolar macrophage cell line, we showed that this chaperone response could be attributed to metformin's ability to inhibit complex I. It is possible that this response is further attributable to the activation of AMPK, although others have reported that AMPK activation results in downregulation of proteostasis genes (Dai et al., 2015).

Our findings may have implications for humans. For example, in a recent study of people residing in an area of China with high levels of PM exposure, treatment with a respiratory filter to reduce PM exposure resulted in decreased levels of oxidative stress, C-reactive protein (CRP) and fibrinogen (both transcriptional targets of IL-6), and catecholamines, thereby validating key components of the mouse model we used in this study (Li et al., 2017). Our finding that metformin prevented PM-induced IL-6 release from human alveolar macrophages supports a similar trial with metformin in high-risk individuals, particularly given its low cost and safety. In addition, the finding that metformin reduces PM-induced IL-6 release may partially explain the association between metformin use and reduced levels of CRP and cardiovascular risk observed in patients with type 2 diabetes (Maruthur et al., 2016). Consistent with this hypothesis, IL-6 and CRP have both been identified as independent risk factors for the development of ischemic cardiovascular disease, and the administration of an inhibitor of IL-1β reduced IL-6 levels, CRP, and cardiovascular risk in a recent randomized clinical trial (Ridker, 2016; Ridker et al., 2017). Furthermore, the unexpected finding that metformin activated proteostasis genes and inhibited inflammation might explain some of the protection against age-related phenotypes in mice administered metformin and provide an additional rationale for proposed studies to administer metformin to humans to prevent the accumulation of age-related phenotypes (Barzilai et al., 2016).

Limitations of Study

First, the dose of metformin we used in mice achieves plasma/tissue concentrations similar to those measured in humans on standard treatment doses for type 2 diabetes (Chandel et al., 2016), but it is not known if metformin is effectively taken up by human alveolar macrophages *in vivo*. Second, we used urban PM obtained from the air around our laboratories in Chicago, and from the National Institute of Standards and Technology from air in Washington, DC, both of which have been characterized (Mutlu et al., 2018; Poster et al., 1999). As the epidemiologic link between PM exposure and cardiovascular disease is not dependent on geography, our results are likely to be broadly applicable (Lelieveld et al., 2015). Nevertheless, it is possible PM from some regions may act via additional mechanisms. Third, the Cre driver we used to delete *Tfam* and *Orai1* in alveolar macrophages also targets dendritic cells in the lung. This is perhaps less important for *Tfam*, which only affects mitochondrial biogenesis, as tissue-resident alveolar macrophages persist for months without input from the bone marrow, while both CD11b+ and CD103+ dendritic cells turn over relatively rapidly (1–2 weeks) in the lung (Misharin et al., 2014, 2017). Fourth, the loss of TFAM in macrophages will impair ATP production, depolarize the mitochondrial membrane, and reduce the supply of metabolic intermediates, among other effects. Therefore, our results using these animals should be interpreted in the context of our *in vitro* and *in vivo* studies. Fifth, our data using the inhibitor U73122 implicate activation of PLC by mitochondrial ROS when PM are present in the depletion of calcium from ER stores and activation of CRAC channels. The precise molecular targets of mitochondrial ROS and PM in this pathway, however, are not known. Finally, while we show the administration of PM results in rapid (<2 min) generation of mitochondrial ROS, dissecting the precise molecular mechanisms by which this occurs will require further study.

STAR★METHODS

Detailed methods are provided in the online version of this paper and include the following:

- KEY RESOURCES TABLE
- CONTACT FOR REAGENT AND RESOURCE SHARING
- EXPERIMENTAL MODEL AND SUBJECT DETAILS
  - Human Subjects
  - Mouse Models
  - Murine Model of PM Exposure
  - Murine Model of Arterial Thrombosis Induced by $FeCl_3$ Injury to the Carotid Artery
  - Murine Alveolar Macrophages and Cell Lines
- METHOD DETAILS
  - IL-6 Measurements
  - Measurement of the NAD^+/NADH Ratio and Metabolomics in Primary Alveolar Macrophages
  - Measurement of Mitochondrial ROS Using MitoSOX and Intracellular Calcium Imaging with Fura-2
  - Isolation of Human Alveolar Macrophages
  - Transcriptome Profiling via mRNA-Seq
  - Metabolomic Analysis
  - Phenotyping and Isolation of the Immune Cells in the Murine Lungs via Flow Cytometry and Cell Sorting
  - Quantitative RT-PCR
- QUANTIFICATION AND STATISTICAL ANALYSIS
  - Statistics
- DATA AND SOFTWARE AVAILABILITY

SUPPLEMENTAL INFORMATION

Supplemental Information includes six figures and one table and can be found with this article online at https://doi.org/10.1016/j.cmet.2018.09.019.

ACKNOWLEDGMENTS

A.V.M.: NHLBI HL135124, NIH NIAMS AR061593, ATS/Scleroderma Foundation Research Grant, DOD grant PR141319, and BD Bioscience Immunology Research Grant. P.A.R.: HL076139. A.B.: NIH HL125940 and the Thoracic Surgery Foundation, Society of University Surgeons, John H. Gibbon Jr. Research Scholarship from American Association of Thoracic Surgery. B.D.J.: HL128867, Parker B. Francis Research Opportunity Award. J.I.S.: NIH AG049665, HL048129, HL071643, HL085534. G.M.M.: NIH ES015024 and ES025644 and ES026718. K.R.: NIH HL079190 and HL124664. G.R.S.B.: NIH ES013995, HL071643, AG049665, VA BX000201, DOD PR141319. H.P.: NIH AR064546, AG049665 HL134375 and the Mabel Greene Myers Chair. N.S.C.: NIH grants AG049665, HL071643, CA197532. Core Facilities (Flow Cytometry and Genomics NCI Cancer Center Support Grant P30 CA060553), the Feinberg School of Medicine, the Center for Genetic Medicine, and Feinberg's Department of Biochemistry and Molecular Genetics, the Office of the Provost, the Office for Research, and Northwestern Information Technology, and maintained and developed by Feinberg IT and Research Computing Group.

AUTHOR CONTRIBUTIONS

Conceptualization, G.R.S.B., G.M.M., A.V.M., M.P., N.S.C., W.E.B., and R.I.M.; Methodology, A.V.M., K.M.R., and S.S.; Investigation, A.J., L.M.N., A.C.M., T.C., R.B.H., A.Y.M., K.A.S., P.S.W., S.E.C., J.M.M., C.I.C., M.C., S.C., and F.J.G.; Resources, M.A., H.A.V., A.B., S.M.B., M.J., and A.G.; Data Curation, H.A.V. and A.V.M.; Writing – Review & Editing, G.R.S.B., N.S.C., G.M.M., A.V.M., W.E.B., M.P., H.P., and R.I.M.; Visualization, S.S., G.R.S.B., and N.S.C.; Supervision, G.R.S.B., G.M.M., S.S., and A.V.M.; Project Administration and Funding, G.R.S.B. and G.M.M.

DECLARATION OF INTERESTS

The authors declare no competing interests.

Received: December 4, 2017
Revised: July 11, 2018
Accepted: September 17, 2018
Published: October 11, 2018

REFERENCES

Barzilai, N., Crandall, J.P., Kritchevsky, S.B., and Espeland, M.A. (2016). Metformin as a tool to target aging. Cell Metab. *23*, 1060–1065.

Batandier, C., Guigas, B., Detaille, D., El-Mir, M.Y., Fontaine, E., Rigoulet, M., and Leverve, X.M. (2006). The ROS production induced by a reverse-electron flux at respiratory-chain complex 1 is hampered by metformin. J. Bioenerg. Biomembr. *38*, 33–42.

Bharat, A., Bhorade, S.M., Morales-Nebreda, L., McQuattie-Pimentel, A.C., Soberanes, S., Ridge, K., DeCamp, M.M., Mestan, K.K., Perlman, H., Budinger, G.R., et al. (2016). Flow cytometry reveals similarities between lung macrophages in humans and mice. Am. J. Respir. Cell Mol. Biol. *54*, 147–149.

Brand, M.D., Goncalves, R.L.S., Orr, A.L., Vargas, L., Gerencser, A.A., Jensen, M.B., Wang, Y.T., Melov, S., Turk, C.N., Matzen, J.T., et al. (2016). Suppressors of superoxide-H(2)O(2) production at site I(Q) of mitochondrial complex I protect against stem cell hyperplasia and ischemia-reperfusion injury. Cell Metab. *24*, 582–592.

Brehme, M., Voisine, C., Rolland, T., Wachi, S., Soper, J.H., Zhu, Y., Orton, K., Villella, A., Garza, D., Vidal, M., et al. (2014). A chaperome subnetwork safeguards proteostasis in aging and neurodegenerative disease. Cell Rep. *9*, 1135–1150.

Bridges, H.R., Jones, A.J., Pollak, M.N., and Hirst, J. (2014). Effects of metformin and other biguanides on oxidative phosphorylation in mitochondria. Biochem. J. *462*, 475–487.

Chandel, N.S., Avizonis, D., Reczek, C.R., Weinberg, S.E., Menz, S., Neuhaus, R., Christian, S., Haegebarth, A., Algire, C., and Pollak, M. (2016). Are metformin doses used in murine cancer models clinically relevant? Cell Metab. *23*, 569–570.

Chiarella, S.E., Soberanes, S., Urich, D., Morales-Nebreda, L., Nigdelioglu, R., Green, D., Young, J.B., Gonzalez, A., Rosario, C., Misharin, A.V., et al. (2014). beta(2)-Adrenergic agonists augment air pollution-induced IL-6 release and thrombosis. J. Clin. Invest. *124*, 2935–2946.

Dai, S., Tang, Z., Cao, J., Zhou, W., Li, H., Sampson, S., and Dai, C. (2015). Suppression of the HSF1-mediated proteotoxic stress response by the metabolic stress sensor AMPK. EMBO J. *34*, 275–293.

Di, Q., Wang, Y., Zanobetti, A., Wang, Y., Koutrakis, P., Choirat, C., Dominici, F., and Schwartz, J.D. (2017). Air pollution and mortality in the Medicare population. N. Engl. J. Med. *376*, 2513–2522.

Duch, M.C., Budinger, G.R.S., Liang, Y.T., Soberanes, S., Urich, D., Chiarella, S.E., Campochiaro, L.A., Gonzalez, A., Chandel, N.S., Hersam, M.C., et al. (2011). Minimizing oxidation and stable nanoscale dispersion improves the biocompatibility of graphene in the lung. Nano Lett. *11*, 5201–5207.

Eden, E., Navon, R., Steinfeld, I., Lipson, D., and Yakhini, Z. (2009). GOrilla: a tool for discovery and visualization of enriched GO terms in ranked gene lists. BMC Bioinformatics *10*, 48.

Fisher, R.P., Lisowsky, T., Parisi, M.A., and Clayton, D.A. (1992). DNA wrapping and bending by a mitochondrial high mobility group-like transcriptional activator protein. J. Biol. Chem. *267*, 3358–3367.

Hamanaka, R.B., Glasauer, A., Hoover, P., Yang, S., Blatt, H., Mullen, A.R., Getsios, S., Gottardi, C.J., DeBerardinis, R.J., Lavker, R.M., et al. (2013). Mitochondrial reactive oxygen species promote epidermal differentiation and hair follicle development. Sci. Signal. *6*, ra8.

Hofmann, T., Obukhov, A.G., Schaefer, M., Harteneck, C., Gudermann, T., and Schultz, G. (1999). Direct activation of human TRPC6 and TRPC3 channels by diacylglycerol. Nature *397*, 259.

Jairaman, A., Maguire, C.H., Schleimer, R.P., and Prakriya, M. (2016). Allergens stimulate store-operated calcium entry and cytokine production in airway epithelial cells. Sci. Rep. *6*, 32311.

Jairaman, A., Yamashita, M., Schleimer, R.P., and Prakriya, M. (2015). Store-operated Ca2+ release-activated Ca2+ channels regulate PAR2-activated Ca2+ signaling and cytokine production in airway epithelial cells. J. Immunol. *195*, 2122–2133.

Lelieveld, J., Evans, J.S., Fnais, M., Giannadaki, D., and Pozzer, A. (2015). The contribution of outdoor air pollution sources to premature mortality on a global scale. Nature *525*, 367.

Li, H., Cai, J., Chen, R., Zhao, Z., Ying, Z., Wang, L., Chen, J., Hao, K., Kinney, P.L., Chen, H., et al. (2017). Particulate matter exposure and stress hormone levels: a randomized, double-blind, crossover trial of air purification. Circulation *136*, 618–627.

Liu, X., Romero, I.L., Litchfield, L.M., Lengyel, E., and Locasale, J.W. (2016). Metformin targets central carbon metabolism and reveals mitochondrial requirements in human cancers. Cell Metab. *24*, 728–739.

Longo, V.D., Antebi, A., Bartke, A., Barzilai, N., Brown-Borg, H.M., Caruso, C., Curiel, T.J., de Cabo, R., Franceschi, C., Gems, D., et al. (2015). Interventions to slow aging in humans: are we ready? Aging Cell *14*, 497–510.

Ma, A., Wang, D., An, Y., Fang, W., and Zhu, H. (2017). Comparative transcriptomic analysis of mice liver treated with different AMPK activators in a mice model of atherosclerosis. Oncotarget *8*, 16594–16604.

Martin-Montalvo, A., Mercken, E.M., Mitchell, S.J., Palacios, H.H., Mote, P.L., Scheibye-Knudsen, M., Gomes, A.P., Ward, T.M., Minor, R.K., Blouin, M.J., et al. (2013). Metformin improves healthspan and lifespan in mice. Nat. Commun. *4*, 2192.

Maruthur, N.M., Tseng, E., Hutfless, S., Wilson, L.M., Suarez-Cuervo, C., Berger, Z., Chu, Y., Iyoha, E., Segal, J.B., and Bolen, S. (2016). Diabetes

medications as monotherapy or metformin-based combination therapy for type 2 diabetes. Ann. Intern. Med. *164*, 750–751.

McNally, B.A., Somasundaram, A., Yamashita, M., and Prakriya, M. (2012). Gated regulation of CRAC channel ion selectivity by STIM1. Nature *482*, 241–245.

Misharin, A.V., Cuda, C.M., Saber, R., Turner, J.D., Gierut, A.K., Haines, G.K., 3rd, Berdnikovs, S., Filer, A., Clark, A.R., Buckley, C.D., et al. (2014). Nonclassical Ly6C(-) monocytes drive the development of inflammatory arthritis in mice. Cell Rep. *9*, 591–604.

Misharin, A.V., Morales-Nebreda, L., Mutlu, G.M., Budinger, G.R.S., and Perlman, H. (2013). Flow cytometric analysis of the macrophages and dendritic cell subsets in the mouse lung. Am. J. Respir. Cell Mol. Biol. *49*, 503–510.

Misharin, A.V., Morales-Nebreda, L., Reyfman, P.A., Cuda, C.M., Walter, J.M., McQuattie-Pimentel, A.C., Chen, C.-I., Anekalla, K.R., Joshi, N., Williams, K.J.N., et al. (2017). Monocyte-derived alveolar macrophages drive lung fibrosis and persist in the lung over the life span. J. Exp. Med. *214*, 2387–2404.

Mutlu, G.M., Green, D., Bellmeyer, A., Baker, C.M., Burgess, Z., Rajamannan, N., Christman, J.W., Foiles, N., Kamp, D.W., Ghio, A.J., et al. (2007). Ambient particulate matter accelerates coagulation via an IL-6 dependent pathway. J. Clin. Invest. *117*, 2952–2961.

Mutlu, E.A., Comba, I.Y., Cho, T., Engen, P.A., Yazici, C., Soberanes, S., Hamanaka, R.B., Nigdelioglu, R., Meliton, A.Y., Ghio, A.J., et al. (2018). Inhalational exposure to particulate matter air pollution alters the composition of the gut microbiome. Environ. Pollut. *240*, 817–830.

Nel, A. (2005). Atmosphere. Air pollution-related illness: effects of particles. Science *308*, 804–806.

Orr, A.L., Vargas, L., Turk, C.N., Baaten, J.E., Matzen, J.T., Dardov, V.J., Attle, S.J., Li, J., Quackenbush, D.C., Goncalves, R.L., et al. (2015). Suppressors of superoxide production from mitochondrial complex III. Nat. Chem. Biol. *11*, 834–836.

Pope, C.A., III, Ezzati, M., and Dockery, D.W. (2009). Fine-particulate air pollution and life expectancy in the United States. N. Engl. J. Med. *360*, 376–386.

Poster, D.L., Schantz, M.M., Wise, S.A., and Vangel, M.G. (1999). Analysis of urban particulate standard reference materials for the determination of chlorinated organic contaminants and additional chemical and physical properties. Fresenius J. Anal. Chem. *363*, 380–390.

Ridker, P.M. (2016). From C-reactive protein to interleukin-6 to interleukin-1: moving upstream to identify novel targets for atheroprotection. Circ. Res. *118*, 145–156.

Ridker, P.M., Everett, B.M., Thuren, T., MacFadyen, J.G., Chang, W.H., Ballantyne, C., Fonseca, F., Nicolau, J., Koenig, W., Anker, S.D., et al. (2017). Antiinflammatory therapy with canakinumab for atherosclerotic disease. N. Engl. J. Med. *377*, 1119–1131.

Semmler-Behnke, M., Takenaka, S., Fertsch, S., Wenk, A., Seitz, J., Mayer, P., Oberdorster, G., Kreyling, W.G., Semmler-Behnke, M., Takenaka, S., et al. (2007). Efficient elimination of inhaled nanoparticles from the alveolar region: evidence for interstitial uptake and subsequent reentrainment onto airways epithelium. Environ. Health Perspect. *115*, 728–733.

Seo, B.B., Kitajima-Ihara, T., Chan, E.K., Scheffler, I.E., Matsuno-Yagi, A., and Yagi, T. (1998). Molecular remedy of complex I defects: rotenone-insensitive internal NADH-quinone oxidoreductase of *Saccharomyces cerevisiae* mitochondria restores the NADH oxidase activity of complex I-deficient mammalian cells. Proc. Natl. Acad. Sci. U S A *95*, 9167–9171.

Somasundaram, A., Shum, A.K., McBride, H.J., Kessler, J.A., Feske, S., Miller, R.J., and Prakriya, M. (2014). Store-operated CRAC channels regulate gene expression and proliferation in neural progenitor cells. J. Neurosci. *34*, 9107–9123.

Subramanian, A., Tamayo, P., Mootha, V.K., Mukherjee, S., Ebert, B.L., Gillette, M.A., Paulovich, A., Pomeroy, S.L., Golub, T.R., Lander, E.S., et al. (2005). Gene set enrichment analysis: a knowledge-based approach for interpreting genome-wide expression profiles. Proc. Natl. Acad. Sci. U S A *102*, 15545–15550.

Vaeth, M., Zee, I., Concepcion, A.R., Maus, M., Shaw, P., Portal-Celhay, C., Zahra, A., Kozhaya, L., Weidinger, C., Philips, J., et al. (2015). Ca2+ signaling but not store-operated Ca2+ entry is required for the function of macrophages and dendritic cells. J. Immunol. *195*, 1202–1217.

Wheaton, W.W., Weinberg, S.E., Hamanaka, R.B., Soberanes, S., Sullivan, L.B., Anso, E., Glasauer, A., Dufour, E., Mutlu, G.M., Budigner, G.S., et al. (2014). Metformin inhibits mitochondrial complex I of cancer cells to reduce tumorigenesis. Elife *3*, e02242.

WHO Regional Office for Europe. (2013). Review of Evidence on Health Aspects of Air Pollution - REVIHAAP Project: Technical Report (WHO Regional Office for Europe).

STAR★METHODS

KEY RESOURCES TABLE

REAGENT or RESOURCE	SOURCE	IDENTIFIER
Antibodies		
CD45 – FITC	BD Biosciences	553080; RRID: AB_394610
CD64 – PE	BioLegend	139304; RRID: AB_10612740
Ly6G – Alexa Fluor 700	BioLegend	127622; RRID: AB_10643269
NK1.1 – Alexa Fluor 700	BioLegend	108730; RRID: AB_2291262
Siglec F – PECF594	BD Biosciences	562757; RRID: AB_2687994
CD11b – APCCy7	BioLegend	101222; RRID: AB_493705
Ly-6C – eFluor 450	Thermo Fisher Scientific	48-5932-82; RRID: AB_10805519
CD24 – APC	BioLegend	101814; RRID: AB_439716
CD11c – PECy7	BD Biosciences	558079; RRID: AB_647251
CD45 – BB515	BD Biosciences	564585; RRID: AB_2732068
CD15 – Alexa Fluor 700	BioLegend	301920; RRID: AB_2728239
HLA-DR – eFluor 450	Thermo Fisher Scientific	48-9952-42; RRID: AB_1603291
CD206 – PE	BioLegend	321106; RRID: AB_571911
CD169 – APC	BioLegend	346008; RRID: AB_11147948
Orai1	Cell Signaling Technology	3280
Chemicals, Peptides, and Recombinant Proteins		
eFluor 506 viability dye	Thermo Fisher Scientific	65-0866-18
Metformin Hydrochloride	Sigma	PHR1084-500MG
Ferric Chloride	Sigma	451649
Particulate Matter	National Institute of Standards and Technology (NIST)	SRM 1649a
MitoSOX	Thermo Fisher Scientific	M36008
Critical Commercial Assays		
RNeasy AllPrep DNA/RNA Mini kit	QIAGEN	80204
NEBNext Ultra RNA Library Prep Kit for Illumina	New England Biolabs	E7530L
IL6 Elisa kit	Invitrogen/Thermo Fisher Scientific	KMC0062
NAD/NADH quantification kit	Sigma	MAK037-1KT
Deposited Data		
Raw and processed data	This paper	GEO: GSE98731
Experimental Models: Cell Lines		
MH-S	ATCC	CRL-2019
Experimental Models: Organisms/Strains		
Tfam$^{flox/flox}$ mice	Navdeep Chandel	Hamanaka et al., 2013
Orai1$^{flox/flox}$ mice	Amgen	Somasundaram et al., 2014
Cre^{CD11c}	The Jackson Laboratory	Strain 008068
C57Bl/6 mice	The Jackson Laboratory	Strain 000664
Oligonucleotides		
IL6 FW	IDT	TTCCATCCAGTTGCCTTCTTGG
IL6 RV	IDT	TTCTCATTTCCACGATTTCCCAG
TFAM FW	IDT	CCAAAAAGACCTCGTTCAGC
TFAM RV	IDT	ATGTCTCCGGATCGTTTCAC

(*Continued on next page*)

Continued

REAGENT or RESOURCE	SOURCE	IDENTIFIER
Recombinant DNA		
Orai1 ShRNA	Sigma Mission	TRCN0000125405
Stim 1 ShRNA	Sigma Mission	TRCN0000193400
Scrambled control ShRNA	Sigma Mission	SHC312
Software and Algorithms		
FlowJo V9.9.4	TreeStar, FlowJo, Ashland, Oregon	https://www.flowjo.com/solutions/flowjo/downloads
GraphPad Prism 6	GraphPad Software, California	https://www.graphpad.com/scientific-software/prism/
bcl2fastq 2.17.1.14	Illumina, California	https://support.illumina.com/sequencing/sequencing_software/bcl2fastq-conversion-software.html
TopHat 2.1.0	Center for Computational Biology at Johns Hopkins University	https://ccb.jhu.edu/software/tophat/index.shtml
HTSeq 0.7.1	Genome Biology Unit, EMBL Heidelberg	https://htseq.readthedocs.io/en/release_0.10.0/
edgeR 3.14.0	Bioconductor	https://bioconductor.org/packages/release/bioc/html/edgeR.html
GENE-E 3.0.215	Broad Institute	https://software.broadinstitute.org/GENE-E/
GOrilla	Eden et al., 2009	http://cbl-gorilla.cs.technion.ac.il/
Other		
Dulbecco's modified Eagle's medium (DMEM)	Fisher Scientific	MT-10-013-CM
Mediatech Cellgro RPMI 1640 medium	Fisher Scientific	MT-10-040-CM
Fetal bovine serum	Omega	FB-01
MEM non-essential amino acids solution (NEAA)	Invitrogen/Gibco	11140-050
L-Glutamine	Invitrogen/Gibco	25030-081
Dulbecco's modified Eagle's medium: nutrient mixture F-12 (DMEM/F-12)	Invitrogen	11330-057
StemPro hESC SFM—human embryonic stem cell culture medium (StemPro medium)	Invitrogen	A1000701
DMEM/F-12 with GlutaMAX	Invitrogen	10565-018
StemPro hESC supplement	Invitrogen	A10006-01
bovine serum albumin (BSA)	Invitrogen	A10008-01
2-Mercaptoethanol	Sigma-Aldrich	M6250
Basic fibroblast growth factor (bFGF)	R&D Systems	233-FB
XF calibrant solution	Seahorse Bioscience	100840-000
XF assay medium	Seahorse Bioscience	100965-000
Bio-Rad protein assay dye reagent concentrate	Bio-Rad Laboratories	500-0006
Carbonyl cyanide 3-chlorophenylhydrazone (CCCP)	Sigma-Aldrich	C2759
Rotenone	Sigma-Aldrich	R8875
Antimycin A	Sigma-Aldrich	A8674
Synta-66	GlaxoSmithKline	Not available, gift
MitoSox	Thermo Fisher Scientific	M36008
Fura-2	Thermo Fisher Scientific	F1221
MitoTempo	Sigma-Aldrich	SML6737
MitoPQ	Abcam	ab146819
U769662	Cayman Chemicals	11900
U73343	Sigma-Aldrich	U6881
U73122	Sigma-Aldrich	U6756
Piericidin A	Sigma-Aldrich	P4368

CONTACT FOR REAGENT AND RESOURCE SHARING

Further information and requests for resources and reagents should be directed to and will be fulfilled by the Lead Contact: Scott Budinger (s-buding@northwestern.edu).

EXPERIMENTAL MODEL AND SUBJECT DETAILS

Human Subjects

All studies using samples obtained from human subjects were approved by the Northwestern University Institutional Review Board. All human subjects provided written informed consent prior to enrolment into the study. The following inclusion criteria were applied: donor lung is suitable for transplant, recipient provided written informed consent, sufficient amount of tissue was provided for isolation of alveolar macrophages. Information about donor's sex, heath status, previous exposure to metformin or other drugs is not available.

Mouse Models

All animal experiments and procedures were performed according to protocols approved by the Institutional Animal Care and Use Committee at Northwestern University. C57BL/6J mice were bred in our facility and our colonies are refreshed yearly with mice purchased from the Jackson Laboratory. Cre^{CD11c} mice were purchased from the Jackson Laboratory and bred in house. $Tfam^{fl/fl}$ mice were generated by Ozgene as we have previously described (Hamanaka et al., 2013). $Orai1^{fl/fl}$ mice were provided by Amgen and generated as described (Somasundaram et al., 2014). All experiments were performed with littermate controls. Number of animals per group was determined based on our previous publications. Ten- to sixteen-week-old male mice were used for experiments. Investigators were not blinded to the group allocation. Mice were housed at the Center for Comparative Medicine at Northwestern University, in microisolator cages, with standard 12 hr light/darkness cycle, ambient temperature 23°C and were provided standard rodent diet (Envigo/Teklad LM-485) and water *ad libitum*.

Murine Model of PM Exposure

Inhalational exposure to $PM_{2.5}$ CAPs was performed as previously described (Chiarella et al., 2014). Briefly, mice were housed 8 hr per day for 3 consecutive days in a chamber connected to a Versatile Aerosol Concentration and Exposure System (VACES). We exposed control mice to filtered air in an identical chamber connected to the VACES in which a Teflon filter was placed on the inlet valve to remove all particles. We estimated ambient $PM_{2.5}$ concentrations as the mean of reported values from the 4 EPA monitoring locations closest to our location. The mean concentration in the PM exposure chamber was 118.3 ± 5.21 μg/m^3. For intratracheal exposure experiments in mice, we used an urban PM collected from ambient air in Washington, DC (National Institute of Standards and Technology standard reference material, SRM 1649a). We instilled either PM suspended in 50 μl of sterile PBS (vortexed prior to instillation) or PBS (control).

Murine Model of Arterial Thrombosis Induced by $FeCl_3$ Injury to the Carotid Artery

This technique has been previously described in detail (Chiarella et al., 2014). Briefly, mice were anesthetized and the left carotid artery was dissected and isolated from the surrounding tissue with paraffin; the adventitia of the artery was treated with Whatman filter paper of a standard size (generated with a mouse ear punch device) soaked in freshly prepared 10% $FeCl_3$. The carotid blood flow was continuously measured using Transonic TS420 Transit-Time Perivascular Flowmeter (Transonic Systems). The application of $FeCl_3$ led to a 2- to 3 mm-long carotid thrombus.

Murine Alveolar Macrophages and Cell Lines

The murine alveolar macrophage cell line (MH-S, ATCC CRL-2019, originating from male BALB/c mouse) was cultured in RPMI medium in 10% FBS supplemented with 10 μM β-mercaptoethanol at 37°C and 5% CO_2. Cell culture and generation of MHS cells with stable knockdown of *Orai1*, *Stim1* or a scrambled shRNA control were performed using the Sigma mission lentiviral packaging mix (Sigma-Aldrich) with the following catalog numbers: ORAI1 (TRCN0000125405), STIM1 (TRCN0000193400), non-target control (SHC312). Transformed cells were cultured with 10 μg/ml puromycin for 2 passages and reduction in the expression of the target gene was assessed using western blot or RT-PCR.

Mouse primary alveolar macrophages were isolated by bronchoalveolar lavage performed in euthanized mice with 3 ml of PBS with 1 mM EDTA. Only male mice were used as a source of alveolar macrophages. The lavage was centrifuged at 300 *g* for 10 min and resuspended in RPMI supplemented with 10% FBS and plated in a density of 100,000 cells/cm^2. Cell purity was analyzed by flow cytometry and was confirmed to be >95%.

METHOD DETAILS

IL-6 Measurements

The production of IL-6 in broncheoalveolar lavage fluid on the lung of mice exposed to particulate matter, and *In vitro* IL-6 production in human alveolar macrophages was determined by ELISA using a kit (ThermoFisher cat# KHC0061 and KMC0061) as previously described (Mutlu et al., 2007).

Measurement of the NAD$^+$/NADH Ratio and Metabolomics in Primary Alveolar Macrophages

The NAD+/NADH ratio in alveolar macrophages was measured using two methods. For both methods, mice were treated with metformin in their drinking water for three days and BAL macrophages were harvested by gently BAL through a surgically placed tracheostomy tube (6 sequential lavages) in PBS containing (0.5 mM EDTA). The cell pellet was washed twice in PBS and cells were counted (Cellometer K2, Nexcelon Bioscience). In the first method, 100,000 cells were used for measurement of the NAD$^+$/NADH using an assay kit from Abcam (ab65348) according to the manufacturer's instructions. In the second method, 100,000 cells were resuspended in 75 μL in PBS solution and snap frozen in liquid nitrogen. using. The cell solution was then thawed and centrifuged for 15 min at 20,000g, 4°C. and filtered using a 10-kDa-molecular weight cutoff filter and then split into two. The first half was used to determine total NAD$^+$ (NAD+NADH), and the second half to determine NADH after heating the samples at 333 K for 30 min. The supernatant was collected for LCMS analysis by High-Performance Liquid Chromatography and High-Resolution Mass Spectrometry and Tandem Mass Spectrometry (HPLC-MS/MS). Specifically, system consisted of a Thermo Q-Exactive in line with an electrospray source and an Ultimate3000 (Thermo) series HPLC consisting of a binary pump, degasser, and auto-sampler outfitted with a Xbridge Amide column (Waters; dimensions of 4.6 mm × 100 mm and a 3.5 μm particle size). The mobile phase A contained 95% (vol/vol) water, 5% (vol/vol) acetonitrile, 20 mM ammonium hydroxide, 20 mM ammonium acetate, pH = 9.0; B was 100% Acetonitrile. The gradient was as following: 0 min, 15% A; 3 min, 45% A; 10 min, 60% A; 10.1-11 min, 75% A; 11.1 min, 15% A; 11.1-15 min, 15% A with a flow rate of 400 μL/min. The capillary of the ESI source was set to 275°C, with sheath gas at 45 arbitrary units, auxiliary gas at 5 arbitrary units and the spray voltage at 4.0 kV. In positive/negative polarity switching mode, a selective iron monitoring method for target irons was used and MS1 data were collected at a resolution of 70,000. The automatic gain control (AGC) target was set at 1 X 10^6 and the maximum injection time was 200 ms. The target ions were subsequently fragmented for confirmation purpose, using the higher energy collisional dissociation (HCD) cell set to 30% normalized collision energy in MS2 at a resolution power of 17,500. Sample volumes of 25 μl were injected. Data acquisition and analysis were carried out by Xcalibur 4.0 software and Tracefinder 2.1 software, respectively (both from Thermo Fisher Scientific).

Measurement of Mitochondrial ROS Using MitoSOX and Intracellular Calcium Imaging with Fura-2

Live cell imaging was used to determine changes in intracellular calcium concentration and mitochondrial superoxide production, using the fluorescent probes MitoSOX (2 μM) and Fura-2 (10 μM). Cells were plated in glass plates for 24 hr in HBSS medium, then washed and incubated in Hank's buffer containing 2 μM MitoSOX-Red and 1μg/ml of Fura-2 for 30 min at 37°C in a 5% CO_2 atmosphere. Cells were washed and incubated in Hank's buffer for 30 min in the dark, then mounted in the Olympus DSU Spinning Disc Confocal microscope attached to a perfusion system and perfused with 1 ml/min of HBSS media in a 5% CO_2 atmosphere at 37°C for the duration of the experiment. Investigators were not blinded to the group allocation and treatment. Single-cell [Ca^{2+}]cyt measurements were done according to the protocol described previously (McNally et al., 2012). Image acquisition and analysis was performed using Slidebook (Denver, CO). For data analysis, regions of interest were drawn around single cells, background subtracted, and the F340/F380 intensity ratios were determined for each time point. The F340/F380 intensity ratios were converted to [Ca^{2+}]cyt using the formula:

$$[Ca^{2+}]_{cyt} = \beta * Kd(R-R_{min})/(R_{max}-R)$$

Where R is the F340/F380 fluorescence intensity ratio and R_{max} (= 9.645) and R_{min} (= 0.268) were determined by *in vitro* calibration of Fura-2 pentapotassium salt. β (= 20.236) was determined from the Fmin/Fmax ratio at 380 nm, and Kd is the apparent dissociation constant of Fura-2 binding to Ca^{2+} (135 nmol).

Isolation of Human Alveolar Macrophages

A small biopsy of donor lung tissue was obtained at the time of lung transplantation surgery and used for isolation via FACSorting (Bharat et al., 2016). Briefly, lung tissue was infiltrated with mixture of collagenase and DNase I and digested at 37°C for 30 min, chopped into 2-3 mm pieces with fine scissors and digested for another 15 min. The resulting single cell suspension was passed through the 40 μμm filter, centrifuged, and red blood cells were lysed using BD Pharm Lyse buffer (BD Pharmingen). Following live/dead staining with eFluor506 viability dye (eBioscience/Affymetrix) and incubation with Fc-blocking reagent (Biolegend) cells were incubated with mixture of fluorochrome conjugated antibodies for 30 min. Alveolar macrophages were sorted on BD SORP FACS Aria III instrument in RHLCCC Flow Cytometry Core facility with 100 um nozzle, at 40 psi using MACS buffer as a capture media. Alveolar macrophages were identified as singlets/CD45$^+$/live/CD15$^-$/HLA-DR^{++}/CD206^{++}/CD169$^+$.

The cell pellet was washed and resuspended in 10 ml of RPMI medium with 10% FBS supplemented with penicillin, streptomycin, and amphotericin B. The cells were then counted (hemacytometer; Trypan Blue), and 100,000 cells were plated on Primaria Cell Culture 12-well plates (Corning). The cells were used 24 hr after plating.

Transcriptome Profiling via mRNA-Seq

Mouse alveolar macrophages were isolated via FACSorting at indicated time points. Approximately 100,000 cells were sorted into MACS buffer, immediately pelleted and lysed in RLT Plus buffer supplemented with 2-mercaptoethanol (Qiagen). RNA was isolated using RNeasy Plus kit with genomic DNA removal step. RNA quality was assessed on TapeStation 4200 instrument (Agilent), all samples had RNA integrity number (RIN) over 7. RNA-seq libraries were prepared from 100 ng of total RNA, starting with poly(A) enrichment and followed by NEB Next RNA Ultra I chemistry. Libraries were quantified and assessed on Qubit fluorimeter (Invitrogen) and TapeStation 4200, correspondingly, multiplexed and sequenced on NextSeq 500 instrument (Illumina), 75 bp, single end reads,

to the average sequencing depth of 6x10^6 reads per sample. Over 94% of reads had Q score over 30. Reads were demultiplexed and mapped to mm10 version of the mouse genome using TopHat2 aligner and mapped to the genomic features using HTSeq and counts processed using edgeR package to estimate differentially expressed genes. FDR p value less than 0.05 was used to identify differentially expressed genes. K-means clustering was performed using GENE-E. Gene ontology analysis was performed using GOrilla on two unranked gene lists. The RNA-seq dataset is available at GEO: GSE98731.

Metabolomic Analysis

Mice were treated with metformin in their drinking water for three days and BAL macrophages were harvested by gently BAL through a surgically placed tracheostomy tube (6 sequential lavages) in PBS containing (0.5mM EDTA). The cell pellet was washed twice in PBS and cells were counted (Cellometer K2, Nexcelon Bioscience). The samples were dried using SpeedVac. 50 μl of 50% acetonitrile was added to the tube for reconstitution following by overtaxing for 30 sec. Samples solution was then centrifuged for 15 min @ 20,000g, 4°C. Supernatant was collected for LCMS analysis. Samples were analyzed by High-Performance Liquid Chromatography and High-Resolution Mass Spectrometry and Tandem Mass Spectrometry (HPLC-MS/MS). Specifically, system consisted of a Thermo Q-Exactive in line with an electrospray source and an Ultimate3000 (Thermo) series HPLC consisting of a binary pump, degasser, and auto-sampler outfitted with a Xbridge Amide column (Waters; dimensions of 4.6 mm × 100 mm and a 3.5 μm particle size). The mobile phase A contained 95% (vol/vol) water, 5% (vol/vol) acetonitrile, 20 mM ammonium hydroxide, 20 mM ammonium acetate, pH = 9.0; B was 100% Acetonitrile. The gradient was as following: 0 min, 15% A; 2.5 min, 30% A; 7 min, 43% A; 16 min, 62% A; 16.1-18 min, 75% A; 18-25 min, 15% A with a flow rate of 400 μL/min. The capillary of the ESI source was set to 275°C, with sheath gas at 45 arbitrary units, auxiliary gas at 5 arbitrary units and the spray voltage at 4.0 kV. In positive/negative polarity switching mode, an *m/z* scan range from 70 to 850 was chosen and MS1 data were collected at a resolution of 70,000. The automatic gain control (AGC) target was set at 1 × 10^6 and the maximum injection time was 200 ms. The top 5 precursor ions were subsequently fragmented, in a data-dependent manner, using the higher energy collisional dissociation (HCD) cell set to 30% normalized collision energy in MS2 at a resolution power of 17,500. The sample volumes of 25 μl were injected. Data acquisition and analysis were carried out by Xcalibur 4.0 software and Tracefinder 2.1 software, respectively (both from Thermo Fisher Scientific).

Phenotyping and Isolation of the Immune Cells in the Murine Lungs via Flow Cytometry and Cell Sorting

Identification and isolation of the immune cells by flow cytometry and cell sorting were performed as described previously (Misharin et al., 2013). Briefly, the mice were euthanized and the lungs were perfused through the right ventricle with 10 ml of HBSS with Ca^{2+} and Mg^{2+}, dissected and infiltrated with collagenase and DNase I, chopped into 2-3 mm fragments, transferred into C-tubes (Miltenyi) and subjected to mechanical disintegration using GentleMACS instrument (Miltenyi). The resulting single cell suspension was filtered through 40 um filter, and subjected to CD45-enrichment using corresponding magnetic microbeads (Miltenyi), stained with eFluor506 viability dye, followed by the mixture of fluorescently labeled antibodies. Cell counts were obtained on K2 cell counter (Nexcelom) using acridine orange to discriminate nucleated cells from debris and propidium iodide to discriminate dead cells. Data were acquired on BD LSR II instrument, cell sorting was performed BD SORP FACS Aria III instrument, 100 um nozzle, 40 psi pressure.

Quantitative RT-PCR

We isolated total RNA from mouse lungs, sorted cells or cell cultures using a commercially available system (TRIzol; Invitrogen) and performed qRT-PCR reactions using IQ SYBR Green superscript analyzed on a Bio-Rad IQ5 Real-Time PCR Detection System using the following primer sequences:

IL-6 (5′-TTCCATCCAGTTGCCTTCTTGG-3′, 5′-TTCTCATTTCCACGATTTCCCAG-3′);
TFAM (5′-CCAAAAAGACCTCGTTCAGC-3′, 5′-ATGTCTCCGGATCGTTTCAC-3′);
mRPL19 (5′-GAAGGTCAAAGGGAATGTGTTCAA-3′, 5′-TTTCGTGCTTCCTTGGTCTTAGA-3′)

QUANTIFICATION AND STATISTICAL ANALYSIS

Statistics

We report all data as mean ± SEM. We subjected all data to 1-way ANOVA. When ANOVA indicated a significant difference, we explored individual differences with 2-tailed Student's t test using Bonferroni's correction for multiple comparisons (Prism 6; Graphpad). Statistical methods for RNA-seq analysis above. For metabolomics, 154 detected metabolites in all samples were analyzed using two way ANOVA followed by multiple comparisons using the two stage linear step up procedure of Benjamini, Krieger and Yekutieli with a FDR q value of 0.1. For some assays (RNA-seq, quantitative RT-PCR, murine model of arterial thrombosis) power and sample size were estimated based on our previous work, the observed data met or exceeded these criteria. The statistical parameters and criteria for significance can be found in the figure legends.

DATA AND SOFTWARE AVAILABILITY

The RNA-seq dataset, containing raw and processed data, is available at GEO: GSE98731.